THEORY

POOL FIRE MODEL

DATE: December 2023

This document describes the theory of the pool fire model. The original PHAST 5.2 version of the pool-fire model calculates the flame shape for a liquid hydrocarbon pool fire. The current new model was developed as part of contract C490005 for RIVM. It includes significant extensions to this model, i.e. to non-hydrocarbon liquid pool fires, and to open fires (e.g. open warehouse fire) with user-specified burn rates and fire diameters. It also calculates excess-air entrainment into the fire and it produces data at a transition plane from which the dispersion calculations are initiated by the Unified Dispersion Model (UDM).

No.	Date	Reason for Issue	Prepared by	Verified by	Approved by
1	Aug 1999	Initial draft for review	H. Witlox		
2	Aug 1999	Include comments RIVM	H. Witlox		
3	Sept 2004	Include validation of POLF-EXPS model	A. Oke and H. Witlox	H. Witlox	
4	Feb 2011	6.7 version – effect of bund on pool fire centre	H. Witlox		
5	March 2019	8.2 version – including the two-zone pool fire model	Y Xu	Oke	
6	Sept 2020	Remove chapter regarding link between pool fire and dispersion model	W. Place	J. Pickles	
7	May 2021	Apply new template	D. Vatier		

Date: December 2023

Prepared by: Digital Solutions at DNV

ABSTRACT

A new generalised and extended standalone pool-fire model POLF is developed. In this model the burn-rate and surface-emissive power formulations are modified for a general (not specifically hydrocarbon) compound. In addition alternative formulas for the flame angle and flame height are included and tested. The excess air entrainment into the pool fire is calculated based on a procedure developed by Delichatsios. In addition to liquid pool fires, the model also allows for open fires (e.g. open warehouse fire) with user-specified burn rates and fire diameters.

POLF outputs the compound mass fractions as a function of height along the fire cylinder. In addition, it produces data at a transition plane (compound concentrations, fire diameter, fire tilt angle, location of centre of plane, temperature, velocity), from which the dispersion calculations are initiated by the Unified Dispersion Model (UDM). The location of this plane is given by the so-called 'Froude' flame height, defined by 90% excess-air entrainment. The POLF program can also be linked with the radiation model EXPS to carry out radiation calculations.

An automated procedure is developed using user-friendly Excel spreadsheets. This allows easy input-generation, running/linking and post-processing for the POLF, EXPS and UDM models. It also combines the output and graphics (height, concentration, velocity, temperature, …) for POLF and UDM, into single arrays and graphs. The new spreadsheet also allows for sensitivity analyses via multiple runs.

It is the intention to include the above extended version and automated procedure into future versions of PHAST and SAFETI. Note however that the same above code (however with limited input via special entry points) is also included in PHAST/SAFETI and NEPTUNE (no user-defined burn rate and no availability of excess air entrainment calculations and UDM linking).

Table of contents

1. INTRODUCTION

Recent overviews of fire hazard calculations for hydrocarbon pool fires are given by Mudan and Croce[1], Rew et al.[2], Chapter 7 of the SINTEF handbook on fire calculations[3] and Chapter 6 of the TNO yellow book[4]. Rew et al. produced a validation data set (burning rate, surface emissive power) which they used for the WS Atkins model POOLFIRE6.

The original pool-fire model implemented into PHAST 5.2 and SAFETI 3.41[5] was developed by Cook et al. [6] for hydrocarbon pool fires to predict burn rate, fire geometry, and surface emissive power of the flame. The overview by Mudan and Croce[1] includes most of the theory adopted in this model.

This report describes the generalisation of the above model to non-hydrocarbon pool fires and the modelling of excess air entrainment into the fire. In addition it describes the linking of the pool-fire model POLF with the Unified Dispersion Model UDM for modelling of the smoke dispersion further downwind. It also describes the linking of the model POLF with radiation models for radiation calculations.

Original pool-fire model (PHAST5.2, SAFETI3.41)

Cook et al.[6] describe the calculation of radiation levels from a jet flame, pool fire or BLEVE. The theory for the pool-fire version in the latest version 5.2 of PHAST is documented by Sections 9.16.4, 10.2.1, 10.2.5 and Figure 10.10 in the SAFETI 3.4 Theory Manual. PHAST calculates and outputs radiation information only, i.e. it does not calculate the dispersion of the smoke [dimensions of the smoke plume; the concentration of the combustion products, CO_2 and H_2O for hydrocarbons, P_4O_{10} (and H_3PO_4) for phosphorus].

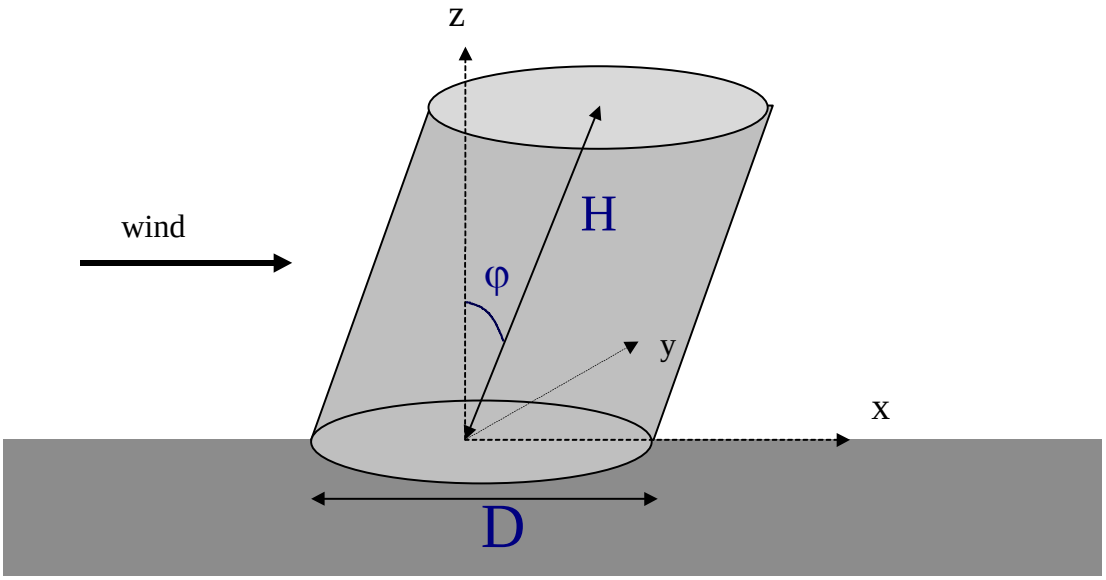

Figure 1. Cartesian co-ordinates x,y,z and pool-fire geometry (diameter D, height H, tilt angle θ)

A cylindrical shape of the pool fire is presumed; see

Figure 1. PHAST first calculates the burn rate, the fire dimensions (tilted cylinder; fire diameter, fire height and tilt angle), and the surface emissive power of the flame. Subsequently it sets the radiation.

The PHAST 5.2 program allows for stand-alone pool-fire modelling for a pool-fire with a user-specified diameter. It also allows for pool-fire calculations to be carried out as part of an accidental scenario, e.g. in case a leak from a vessel leads to the formation of an ignitable liquid pool. First no ignition is assumed, and pool-evaporation and dispersion calculations are being carried out. Subsequent early fires (immediate ignition) or late pool fires (ignition following spreading of liquid pool) are considered.

The validation[i] for the PHAST pool-fire model has been described in Appendix II.4 of the PHAST 4.2 release notes[7] for LNG fires [against data from Johnson (1992) and Nedelka, Moorhouse and Tucker (1990); comparison of measured and calculated radiation contours], hexane fires [against data from Lois and Swithenback] and kerosene fires [against data from Fu (1974) and Uguccioni and Messina]. Based on these results it was suggested that improvements could be made by incorporating flame drag and using an elliptical cross section for the fire rather than a circular one.

Model extension to non-hydrocarbon pool fires and air entrainment

Witlox and Woodward[8,9] modelled phosphorus pool fires and the subsequent smoke dispersion (work sponsored by Albright and Wilson). This involved an extension of the current PHAST pool-fire formulation to non-hydrocarbon fires (e.g. phosphorus). Furthermore the pool-fire formulation was extended to include the calculation of the amount of excess air entrainment as function of height. The pool-fire model produces data at a transition plane, from which the dispersion calculations are initiated.

The pool-fire model POLF calculates the burn rate, radiation levels, fire diameter, fire height, tilt angle, mass fractions [excess air, and each individual compound in the initial combustion product, i.e. combustion-oxide, nitrogen, water and unburned fuel] and temperature as function of height, and transition data at the transition plane. The excess-air entrainment is calculated based on a procedure developed by Delichatsios[10].

The above approach has the following limitations:

- The old automated procedure is running under DOS and uses out-dated graphics software.
- The old procedure is automated for phosphorus only. For any other compounds (e.g. hydrocarbons) the method can only be applied by an expert user, and it requires model extensions. This is a very lengthy process.
- The phosphorus pool-fire model is based on the old 16-bits version of the pool-fire model. The new 32-bits version currently being prepared for PHAST 6.0 does not include the air entrainment formulation.
- The phosphorus UDM model is outdated and specific for phosphorus, and many improvements to the UDM model have been applied afterwards.

For RIVM the above procedure was applied to kerosene fires and the subsequent smoke dispersion[11].

Scope of current work

As a result, the intention of the current work is to eliminate the above shortcomings. It involves the following:

1. To generalise the current 32-bits version of the PHAST 6.0 pool-fire model:

   (a) to allow for 'general' non-hydrocarbon liquid pool fires in addition to non-sooty and sooty hydrocarbon fires

   (b) to allow for 'open' fires, with user-defined burn rates and a fire diameters; a multi-compound fuel can be defined via specifying a mixture in the PHAST/SAFETI material database

   (c) to add air-entrainment, mixture-composition and thermodynamics calculations

2. To develop an automated procedure using user-friendly Excel spreadsheets. This allows easy input-generation, running/linking and post-processing for the POLF, EXPS and UDM models. It also combines the output and graphics (height, concentration, velocity, temperature…) for POLF and UDM, into single arrays and graphs. The new spreadsheet also allows for sensitivity analyses via multiple runs.

2. POOL FIRE MODEL (POLF)

Prior to version 8.2, pool fires were represented in Phast/Safeti by a tilted cylinder with uniform surface emissive power (SEP). A two-zone pool fire model has been introduced in Phast/Safeti 8.2. To differentiate the two pool

[i] DOC - Documentation from PHAST 4.2 release notes to be reviewed and moved to current documentation, with validation input data to be established and data to be rerun.

fire models described in this document, the pool fire model with uniform flame SEP is referred to as “POLF”, while the two-zone pool fire model, as described in section 2.3, is referred to as “POLF-TwoZone”.

2.1 List of input and output data

Use is made of Cartesian co-ordinates x,y,z with x the downwind distance, y the cross-wind distance and z the height above the ground. Input to the model is ambient data, pool data, and fuel properties

Ambient data

The ambient data are assumed to be uniform in the POLF model. These are the wind speed u_a (m/s)[ii], temperature T_a (K), relative humidity r_h (fraction), and the absolute pressure P_a (N/m^2).

Pool data

The pool is located at x = 0, y = 0, z = z_{pool}, where z_{pool} is the vertical elevation (m) of the pool. The spill rate of the liquid fuel into the pool is S_{pool} (kg/s; e.g. due to rainout), and the liquid temperature is T_{pool} (K; used for pool-fire thermodynamics only). In case of the presence of a bund, the bund diameter is D_{bund} ($D_{bund} = \infty$, in absence of bund). Furthermore the pool fire may be located on land or water.

Fuel properties

The user needs to specify the (liquid) fuel material from the material database (e.g. white phosphorus P_4). The material properties needed for the liquid fuel are:

- molecular weight of liquid fuel, M_w (kg/kmol)
- specific heat of liquid at T_b, C_{pL} (J/kg/K)
- liquid density at T_b, ρ_L (kg/m^3)
- boiling temperature, T_b (K)
- heat of vaporisation at T_b, ΔH_v (J/kg)
- vapour density at T_b, ρ_v (kg/m^3)
- characteristic length for increase of burn rate m with diameter D, L_b (m)
- if experimental data are known, a maximum value for burn rate m, M_{max} (kg/m^2/s)
- net heat of combustion at T_b, ΔH_c (J/kg)
- specific heat of combustion oxide, C_{poxi}
- phase of combustion oxide VAPOXI: vapour (VAPOXI=0) or non-vapour (VAPOXI=1; for use in density calculations)
- combustion efficiency χ_A (-; $0<\chi_A<1$); this is the mass fraction of fuel which combusts with the surrounding air (the remaining unburned fuel forms part of the ‘combustion product’)[iii]
- stoichiometric ratio S_{th} (-); this is the mass ratio of dry air to fuel needed for complete combustion; it can be derived from the combustion reaction properties A_t, C_t (see Appendix A).
- flame type FLMTYP[iv]: luminous hydrocarbon (0), smoky hydrocarbon (1), and general (2 - for compounds with unknown experimental profile for surface emissive power)
- radiative fraction χ_R (-):
  - for FLMTYP=2 (general flame type), this parameter is set equal to 0.35 if not user-specified (recommended value by TNO yellow book[4]).
  - for FLMTYP=0,1, χ_R is not needed but is set from known experimental data for the surface-emissive-power profile
- if experimental data are known (FLMTYP=0,1) then:
  - maximum surface emissive power for luminous fires E_m, kW/m^2
  - smoke surface emissive power E_s, kW/m^2 (for sooty fires only; E_s=20kW/m^2 currently always assumed)
  - characteristic length for decay of emissive power E_f with D, L_s (m)

The variables above are summarised in the table below. The table includes the following:

[ii] JUSTIFY. Guidance to be given for reference height for evaluation of ambient wind speed, e.g. by checking original reference for correlations etc. Note that upon UDM linking the ambient data are mapped onto the UDM data at the given reference height. As a result this height has been fixed at 10 m height.

[iii] NOTE. Given deficiencies in the formulation, currently advised to adopt combustion efficiency = 1

[iv] CHECK. To check for appropriate flame type for mixture (what is current mixing rule?)

- the name, symbol and unit for the property

- how the property is obtained:

  - o from values of the DIPPR data bank[12]
  - o from the experimental database (EXPDB)
  - o as user input
  - o as a fixed coded-in value
  - o derived from other material properties

  The DIPPR, EXPDB values are obtained from the PHAST database. If needed, the user may add to this database components and mixtures. Also existing properties can be modified by the user.

- when the property is used [i.e. for what type of flame type; luminous flame (FLMTYP =0), sooty flame (1) or general flame (2)]; the maximum burn rate M_{max} is calculated, if an experimental value is not stored in the database (flagged by M_{max} =0).

- property values specific for white phosphorus (P_4):

  - o The DIPPR values are derived by adjusting the values from the DIPPR databank-values given for P (transfer values for moles of P to moles of P_4).
  - o The value for the specific heat of solid combustion oxide at T_b is derived from DIPPR.
  - o Since the burn-rate characteristic length L_b is not known, the worst-case value L_b=0 is assumed (burn rate is always equal to the maximum burn rate).
  - o The value for the heat of combustion is obtained from the Chemical Safety Data Sheet[13]
  - o See Section 2.3.3 for the calculation of the stoichiometric ratio

property	symbol	unit	reference	when used	P_4	propane (PHAST)	kerosene (ORBIT)
molecular weight	M_w	kg/kmole	DIPPR	always	124	44.	
boiling temperature	T_b	K	DIPPR	always	553.45	231.1	526.7
heat of evaporation	$\Delta H_v(T_b)$	J/kg	DIPPR	always	4E5	4.26E5	2.43E5
liquid specific heat	$C_{pL}(T_b)$	J/kg/K	DIPPR	always	849	2233	3387
liquid density	$\rho_L(T_b)$	kg/m^3	DIPPR	always	1528	582	595
vapour density	$\rho_v(T_b)$	kg/m^3	DIPPR	always	290	2.42	4.93
burn-rate charac. length	L_b	m	EXPDB	always	0(assumed)	2.0	10.0
maximum burn rate	M_{max}	kg/m^2/s	EXPDB	if known	-	0.12	0.039
heat of combustion	ΔH_c	J/kg	EXPDB	always	2.47E7	4.63E7	4.4E7
specific heat comb.oxide	C_{poxi}	J/kg/K	input	always	500	1361.8	1316.7
phase indicator comb.oxide	VAPOXI	-	input	always	1	0	0
combustion efficiency	χ_A	-	input	always	1(assumed)	1 (assumed)	1(assumed)
comb.reaction parameter	A_t	-	EXPDB	always	1.25	0.9612	0.94
comb.reaction parameter	C_t	-	EXPDB	always	0.04	0.040	0.0965
stoichiometric ratio	S_{th}	-	derived	always	5.53	15.6	15
flame type (0,1,2)	FLMTYP	-	EXPDB	always	2 (general)	0(luminous)	1 (sooty)
radiative fraction	χ_R	-	fixed	general	0.35	-	0.4
max. surf. emis. power	E_m	W/m^2	EXPDB	lum.&sooty	-	160E3	140E3
smoke surf. emis. power	E_s	W/m^2	fixed	sooty	-	20E3	20E3
emis. power char. length	L_s	m	EXPDB	lum.&sooty	-	2.75	8.33

Output data:

For 'normal' calculations, the following output data are produced:

1. Scalar flame data:

   - flame length H, m
   - flame diameter D, m
   - tilt angle φ of flame cylinder to vertical, radians
   - surface emissive power E_f, W/m^2
   - radiative fraction χ_R

- burn rate $m_F = (0.25\pi D^2)$ m, kg/s

2. Flame co-ordinates as input to the radiation model. Depending on the selected radiationmodel, the radiation model may calculate radiation data at a given point, as function of downwind distance (along a given line), or contours of radiation levels in a given plane.

3. Data as function of axial distance:

   - total mixture flow m_{tot} (kg/s)
   - mass fractions of mixture compounds (combustion oxide, initial N_2, initial water, unburned fuel, excess wet air)
   - flame temperature (K), mixture density (kg/m^3), flame velocity (m/s)
   - concentration (kg/m^3) and mole fraction of combustion product in mixture

Special calculations

Expert users may wish to specify as input one or more of the above scalar output data. These are the flame length, flame angle, flame diameter, burn rate and surface emissive power. The user may also specify a multi-compound mixture for the fuel.

In case of a user-specified burn rate, these users must also specify the pool diameter.

If the fuel is a multi-compound mixture, the mixture needs to be defined in the usual manner via the PHAST/SAFETI material database. Thus averaged mixture properties (e.g. boiling temperature, molecular weight, combustion reaction factors A_t, C_t) are calculated using mixing rules. See the PHAST/SAFETI documentation for details. The table below includes an example for a mixture of hexane and octane (both 50% mass fraction)

property	hexane	octane	hexane_octane
CAS number	110543	111659	-20 (mixture)
boiling temperature T_b (K)	341.9	398.8	357
molecular weight M_w (kg/kmole)	86.18	114.2	98.24
combustion reaction factor C_t	0.0216	0.0165	0.0194
combustion reaction factor A_t	0.9487	0.9453	0.9470

2.2 Burn rate, fire geometry and surface emissive power of flame

A cylindrical shape of the pool fire is presumed; see
Figure 1.
The burning rate of the liquid fuel, the pool-fire dimensions (diameter, height, tilt angle, flame co-ordinates) and surface emissive power are set by means of the following algorithmic steps.

1. Set input data and material properties (see previous section)

2. Set modified heat of vaporisation (J/kg)[v]:

$$\Delta H_v^* = \Delta H_v + C_{pL}(T_b)\max\{0, T_b - T_a\} \quad (1)$$

3. Set maximum burn rate, m_{max} (kg/m^2/s):

   If the maximum burn rate M_{max} is defined in the property data base ($M_{max} > 0.001$), the maximum burn rate is set as: $m_{max} = M_{max}$. Otherwise it is determined by multiplying the burn velocity (m/s) by the liquid fuel density ρ_L (kg/m^3) leading to [1,14,vi]

[v] JUSTIFY. More accurate: use integration of $C_p(T)dT$ between T_a and T_b. Could this also be set using property routines.

[vi] JUSTIFY. Mudan states that the formula for hydrocarbon fits wider range of hydrocarbon fuels, including liquefied gases. Formula from Grumer et al., which extended formula by Burgess et al. Ideally should these references further be checked regarding validity in general and for phosphorus in specific. The 'general' formula was proposed to be used for phosphorus by Albright & Wilson. This formula is based on extensive experimental data.

$$m_{max} = 1.27 * 10^{-6} \rho_L \frac{\Delta H_c}{\Delta H_v^*} \text{ , general (FLMTYP=2)}$$

$$m_{max} = 10^{-3} \frac{\Delta H_c}{\Delta H_v^*} \text{ , hydrocarbon (FLMTYP=0,1)} \qquad (2)$$

For a pool on water and normal boiling temperature below the ambient temperature, the maximum burn rate as set above is increased with a factor 2.5: $m_{max} = 2.5 * m_{max}$.

4. Set pool-fire diameter D[vii]

- In case of an 'early pool fire' immediate ignition is assumed and the steady-state fire diameter D is calculated by assuming the total burn rate $[\pi D^2/4]m_{max}$ to be equal to the spill rate S_{pool} (kg/s), with the upper bound of diameter (D_{Limit}) being the pool diameter itself if defined or the bund diameter. These limits are applied to avoid excessively large diameters for short duration releases.

$$D = \min \left[D_{Limit} , 2 \sqrt{\frac{S_{pool}}{\pi m_{max}}} \right] \qquad (3)$$

- In case of a 'late pool fire', liquid pool spreading is assumed to take place prior to ignition. For this case the fire diameter is directly input to the model. The fire diameter needs also to be input in case of a user-specified burn rate.

5. Set burn rate m (kg/m^2/s)[viii]:

- The burn rate m asymptotes to its maximum value m_{max} at large diameters[1,2]

$$m = m_{max} \left[1 - e^{-\frac{D}{L_b}} \right] \qquad (4)$$

6. Use the widely adopted and established Thomas[15] correlation to set the flame height in terms of the flame diameter, the burn rate and the ambient density.

$$H = 42 D \left[\frac{m}{\rho_a \sqrt{g D}} \right]^{0.61} \qquad (5)$$

The above formula is used as input for subsequent radiation calculations.

In addition to the above, also results for alternative formulations are output, i.e. Thomas formula including wind-speed effects [see Equation (14) in Reference 1]

$$H = 55 D \left[\frac{m}{\rho_a \sqrt{g D}} \right]^{0.67} (u_*)^{-0.21} \qquad (6)$$

[vii] CHANGED. The old POLF model allowed for early fires (immediate ignition assumed) and late fires (liquid pool spreading assumed to take place before ignition). For early fires the diameter is calculated as described. The late fire logic has been removed from the POLF model. This involved the formula

$D = \min \left[D_{bund} , 2 \sqrt{\frac{M_L}{\pi m_{max} \left(dose_{eq} / dose \right)}} \right]$ with $dose_{eq}$ and dose being radiation intensity and radiation dose, respectively. Now fire diameter is directly input to the pool-fire model in case of late fires.

[viii] JUSTIFY. Note that this equation applies that the burn rate is smaller than the spill rate, with the difference being relatively larger for smaller diameter (e.g. smaller spill rate).

where the non-dimensional wind velocity is given by

$$u_* = u_a \left[\frac{g\, m\, D}{\rho_v} \right]^{-1/3} \qquad (7)$$

with u_a the wind speed (m/s), g the gravitational acceleration (m/s^2), and ρ_v the vapour density of the fuel. Finally a flame height is calculated following a formula by Delichatsios[10] in terms of the Froude number (see Section 2.3 for further details[ix]).

7. Two methods are available for the tilt angle[x]. The first formula is the AGA formula for the tilt angle ϕ[16] :

$$\begin{aligned} \phi &= 0, && u_* \le 1 \\ \phi &= \arccos\left[\frac{1}{\sqrt{u_*}}\right] && u_* > 1 \end{aligned} \qquad (8)$$

The second formula is introduced by Johnson (1992)[17]. For u_a<0.4 m/s, the tilt angle ϕ=0[xi]. Otherwise the tilt angle ϕ is defined by the following equation [see Equation (4) in Johnson (1992)]

$$\frac{\tan\varphi}{\cos\varphi} = A, \quad with \quad A = 0.7 \left(R_e\right)^{0.109} \left(F_r\right)^{0.428}$$

Here the Reynolds number R_e and the Froude number F_r are given by,

$$R_e = \frac{u_a D}{\nu_a}, \quad F_r = \frac{u_a{}^2}{g\, D}$$

where u_a is the wind velocity (m/s), D the flame diameter (m), ν_a the kinematic viscosity of air (m^2/s), and g is the gravitational acceleration (m/s^2).

The above formula can be rewritten as a quadratic equation in sinϕ,

$$A\left[\sin\varphi\right]^2 + \left[\sin\varphi\right] - A = 0$$

with as solution the positive root

$$\varphi = \arcsin\left(\frac{-1+\sqrt{1+4A^2}}{2A} \right)$$

8. The surface emissive power of the flame (W/m^2) is set as

$$\begin{aligned} E_f &= E_m \left[1 - e^{-\frac{D}{L_s}} \right], && \text{luminous fires (FLMTYP=0)} \\ &= E_m \left[e^{-\frac{D}{L_s}} \right] + E_s \left[1 - e^{-\frac{D}{L_s}} \right] && \text{sooty fires (FLMTYP=1)} \end{aligned} \qquad (9)$$

[ix] JUSTIFY - Further investigation of best formula needed? Check e.g. articles on flame height in SFPE handbook. Check if also tested for non-hydrocarbons.

[x] JUSTIFY – The formula for the AGA formula refers to a LPG study. Can we use this for phosphorus? It should also be checked why at a later stage in PHAST, preference is given to the Johnson formula. Did this follow from the validation exercise, or from arguments in Johnson's paper?

[xi] JUSTIFY. To check original paper by Johnson. Why different formulas for u_a<0.4 m/s and u_a>0.4 m/s?

$$= \frac{\chi_R m \Delta H_c}{\left[1+4\frac{H}{D}\right]}, \qquad \text{'general' fire (FLMTYP=2)}^{xii}$$

where E_m is the maximum emissive power for luminous fires, E_s the smoke emissive power[1], and L_s a characteristic length for decay of E_f. If experimental data are not available, the above equation for a 'general fire' is used. This equation is derived from the definition of the radiative fraction χ_R; χ_R is the ratio of the total energy radiated (from the fire surface) to the total energy released (from the pool area):

$$\chi_R = \frac{radiated\ energy}{released\ energy} = \frac{(flame\ surface)*(surface\ emissive\ power)}{(burn\ rate)*(pool\ area)*(heat\ of\ combustion)}$$
$$= \frac{\left[\frac{1}{4}\pi D^2 + \pi\, D\, H\right] E_f}{m\left[\frac{1}{4}\pi D^2\right]\Delta H_c} = \frac{\left[1+4\frac{H}{D}\right] E_f}{m\,\Delta H_c} \qquad (10)$$

2.3 Two-zone pool fire model (POLF-TwoZone)

The surface emissive power of pool fires usually varies with height, particularly for smoky pool fires. Koseki (2000)[18] summarises experimental results involving large pool fires from a significant number of test studies conducted by the author in Japan with pool diameter up to 80m. Infrared images of the tests showed two regions of strong radiant emittance, i.e. a flame base zone and an intermittent flame zone above. The flame base zone emitted strong and steady radiation and the intermittent flame zone was changing with pulsations of the fire. Consequently, most radiation was emitted from the flame base zone. In some of the tests, it was estimated that 70% of the total emitted radiation was from the flame base zone which was less than 25% of the flame height. In general, multi-zone pool fire models seem capable of more accurately representing radiant emittance from pool fires when compared against traditional single zone models and give more accurate radiation predictions in nearfield. For example, pool fires are represented by two radiant zones in Poolfire6 as described by Rew and Hulbert (1996)[2].

The correlations in section 2.2 for flame shape and heat emitted of pool fires are based on empirical data and in general, are adequate for predicting pool fire geometry and radiation at positions far away from the fire, as demonstrated by the validation in Section 4. As such, for the two-zone pool fire model introduced in Phast/Safeti 8.2, flame geometry and total heat emitted off pool fires still employ the correlations given in section 2.2. However, in POLF-TwoZone, the pool flame is represented by a tilted cylinder having 2 radiant zones, i.e. a luminous base zone and a smoky upper zone as shown in Figure 2. Each zone has its own surface emissive power (SEP) with the luminous base zone having a higher SEP when compared against the upper smoky zone. Correlations for flame length of the luminous base zone and SEP for both zones are presented below.

Currently, the two-zone pool fire model is only applicable to smoky pool fires, i.e. pool fires stemming from materials categorized as "smoky" within the Phast/Safeti material property system. For pool

[xii] JUSTIFY. Should the appropriate formula for a general fire, not include term $\chi_a\chi_R$ instead of χ_R?

fires resulting from materials classified as “luminous” or “general”, the single radiant zone model, POLF, is employed.

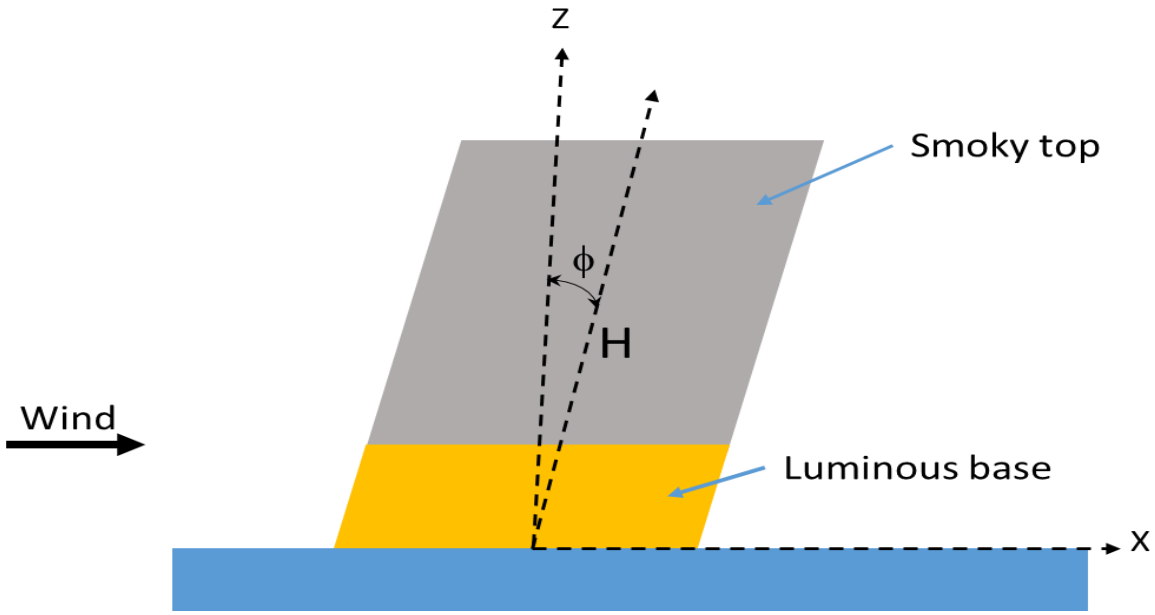

Figure 2 Two-zone pool fire model

Luminous flame length

The pool fire luminous flame Length L_c is calculated using the correlation given by Pritchard & Binding (1992)[19] as:

$$\left(\frac{L_c}{D}\right) = 11.404(\dot{m}'')^{1.13}({U_9}^*)^{0.179}\left(\frac{C}{H}\right)^{-2.49} \quad (11)$$

$$U_9^* = \frac{U_9}{(gmD/\rho_a)^{1/3}}$$

$$\dot{m}'' = \frac{m}{\rho_a(gD)^{1/2}}$$

Where

L_c = Flame length of the luminous base zone.

$\dot{m}''$ = dimensionless burning rate of the fuel.

${U_9}^*$ = dimensionless wind speed at a height of 9m

U_9 = wind speed a height of 9m.

$\frac{C}{H}$ = carbon ratio of the fuel (ratio of number of C to H atoms in molecule)

Note that the "luminous flame length ratio" reported in Phast/Safeti, also referred to as "clear flame length ratio" in some texts, corresponds to the ratio of luminous pool flame length to total flame length.

Surface emissive power of the two zones

The surface emissive power of the two zones differs and are determined as follows:

- Calculate the total heat emitted from the pool fire using the fire geometry (i.e. surface area) and flame SEP calculated using correlations given in section 2.2.
- Determine SEP of the luminous base zone using the correlation for luminous fire as given in equation (9)
- Calculate flame length of the luminous base zone using equation (11)
- SEP of the upper smoky zone is calculated as:

$$SEP\ of\ the\ smoky\ zone = \frac{\boldsymbol{Total\ heat\ emitted - surface\ area\ of\ the\ luminous\ zone * SEP\ of\ the\ luminous\ zone}}{\boldsymbol{surface\ area\ of\ the\ smoky\ zone}} \quad \textbf{(12)}$$

2.4 Excess-air entrainment and mixture composition

The pool-fire excess-air entrainment is taken from correlations by Delichatsios[10]. He derived correlations for air entrainment into turbulent jet flames and pool fires, which were based on experimental data and similarity arguments. He proposed a procedure for calculating air entrainment into turbulent pool and jet fires. He distinguishes between buoyant jet flames, intermediate-scale pool fires and very large pool fires (mass fires).

Delichatsios expresses the excess air entrainment mentr (kg/s) as a function of the ratio Z/D, where Z is the axial height along the flame cylinder and D the flame diameter. This function is expressed in terms of the Froude number Fr and the 'Froude' flame height Hfr, defined to be the height at 90% excess-air entrainment. He distinguishes between the following entrainment zones (
Figure 3):

I. Close to the pool fire: $Z < \min(D, H_{fr})$
II. In or beyond the neck-in area: $D<Z<\min(5D, H_{fr})$
III. Above the neck-in area and below the flame tip: $5D < Z < H_{fr}$
IV. Above the flame tip ($Z>H_{fr}$),

The excess air entrainment is determined for the above zones as follows,

$$Fr\,\frac{m_{entr}}{(1+\chi_a S_{thw})\,m_F} = \begin{cases} 0.086\,(Z/D)^{0.5}, & \text{zone I} \\ 0.093\,(Z/D)^{1.5}, & \text{zone II} \\ 0.018\,(Z/D)^{2.5}, & \text{zone III} \\ 0.21 Fr^{1/3}\,[(Z-H_{fr}+10.21Fr^{0.4})/D]^{5/3}, & \text{zone IV} \end{cases} \qquad (13)$$

where χ_a is the combustion efficiency, S_{thw} the stoichiometric mass ratio of excess-air to fuel, and m_F the mass flow (kg/s) of the initial liquid fuel, $m_F = (0.25\pi D^2)\,m$.

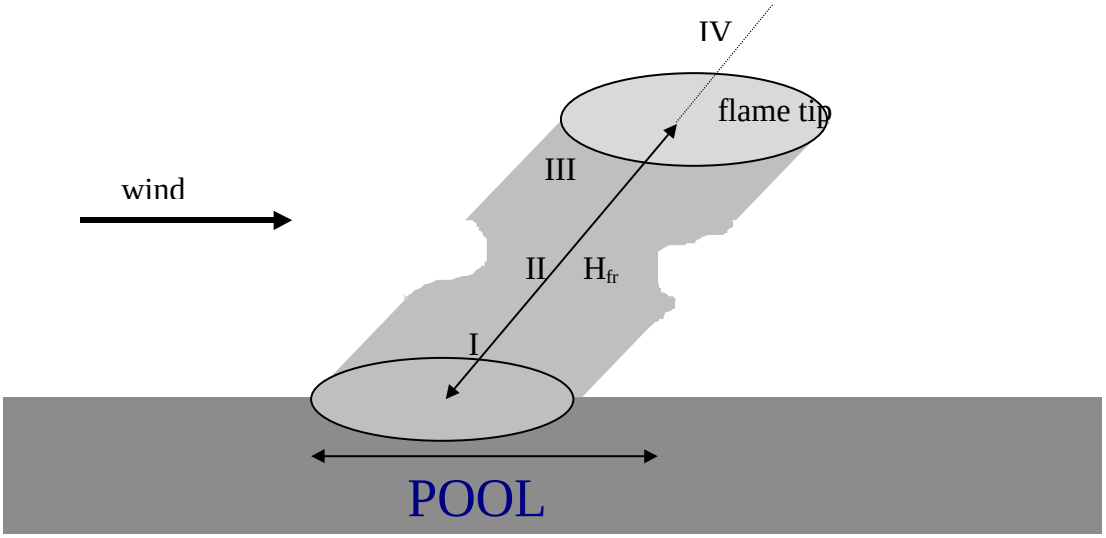

Figure 3. **Pool-fire entrainment zones: I. near pool fire, II. neck-in area, III. below flame tip, IV. above flame tip**

In the remainder part of this section, first expressions proposed by Delichatsios will be given for the Froude flame height H_{fr} and the Froude number Fr. Subsequently the stoichiometric ratio S_{thw} will be calculated from the composition of the ambient moist air, and the stoichiometric dry-air to fuel ratio S_{th}. Finally formulas for the mass fractions of the individual compounds in both the initial combustion product (no excess air) and the final mixture (including excess air) will be derived.

Froude flame height

Following Equation (20) in Reference 10, the Froude flame height H_{fr} is defined to be the height at approximately 90% excess-air entrainment and is given by

$$H_{fr}/D = \begin{cases} 1.35\times10^{4}\,Fr^{2}, & Fr < 8.6\times10^{-3}\ \text{(turbulent jet fire)} \\ 22.54\,Fr^{2/3}, & 8.6\times10^{-3} < Fr < 0.1\ \text{(intermediate-scale pool fire)} \\ 12.52\,Fr^{0.4}, & Fr > 0.1\ \text{(mass pool fire)} \end{cases} \qquad (14)$$

Froude number[xiii]

Following Equations (6), (2), (7) in Reference 10, the dimensionless characteristic fire Froude number Fr is defined by

$$Fr = \frac{(B_\infty/\rho_a)}{D^{2.5}\left[B_T(\chi_a-\chi_R)\right]^{1.5}}, \quad \text{with } B_\infty = \frac{gQ_c}{C_{pa}T_a}, \quad B_T = \frac{g\Delta H_c}{C_{pa}T_a(1+\chi_A S_{thw})} \qquad (15)$$

[xiii] JUSTIFY. A more appropriate term for the convective heat appears to be $Q_c = (1-\chi_R)\chi_a Q$ and also enumerator for Froude number may be incorrect. However this is not changed in order not to possibly invalidate Delichatsios correlations.

Here B_∞ is the maximum buoyancy flow (N/s) at the flame tip, and B_T is the buoyancy term (N/kg) arising from the buoyancy of individual hot eddies burning at the flame temperature; g is the gravitational acceleration (9.81 m/s^2), C_{pa} the specific heat of air (1004 J/kg/K), ρ_a the ambient density (kg/m^3), and T_a the ambient temperature (K). Finally Q_c is the convective heat-release rate (J/s) given by $Q_c = (\chi_a - \chi_R)Q$, with the theoretical heat-release rate $Q = m_F \Delta H_c$.

Composition of ambient moist air

The mole fractions y_w^{wa}, y_{O2}^{wa}, y_{N2}^{wa} of water, oxygen and nitrogen in moist air are given by

$$y_w^{wa} = r_h \frac{P_v^w(T_a)}{P_a}, \quad y_{O2}^{wa} = 0.21(1-y_{wa}), \; y_{N2}^{wa} = 0.79(1-y_{wa}) \qquad (16)$$

where r_h is the relative humidity, P_a the ambient pressure, and $P_v^w(T_a)$ the vapour pressure of water at the ambient temperature T_a. Using that the molar masses for O_2, N_2, H_2O are M_{O2} =32, M_{N2}=28, M_w=18 kg/kmole, it easily follows that the moist air consists of the following mass fractions η_w^{wa}, η_{O2}^{wa}, η_{N2}^{wa} of water, oxygen and nitrogen

$$\eta_w^{wa} = \frac{y_w^{wa}}{1.602(1-y_w^{wa})+y_w^{wa}}, \; \eta_{O2}^{wa} = \frac{0.373(1-y_w^{wa})}{1.602(1-y_w^{wa})+y_w^{wa}}, \; \eta_{N2}^{wa} = \frac{1.229(1-y_w^{wa})}{1.602(1-y_w^{wa})+y_w^{wa}} \qquad (17)$$

Stoichiometric ratio

The stoichometric ratio S_{th} is the mass ratio of dry air to fuel needed for complete combustion; it can be derived from the combustion reaction properties A_t, C_t; see Appendix A for full details (general derivation, and examples for general hydrocarbons and phosphorus).

The theoretical stoichiometric mass ratio S_{thw} is defined to be the mass ratio of wet air needed to the mass of fuel needed in case of complete combustion. From Equation (17) it follows that[xiv]

$$S_{thw} = S_{th} \frac{\eta_w^{wa} + \eta_{O2}^{wa} + \eta_{N2}^{wa}}{\eta_{O2}^{wa} + \eta_{N2}^{wa}} = S_{th} \frac{1.602(1-y_w^{wa})+y_w^{wa}}{1.602(1-y_w^{wa})} \qquad (18)$$

The stoichiometric mass air to fuel ratio $S = \chi_A S_{thw}$, with χ_A being the combustion efficiency. For open hydrocarbon fires with sufficient availability of air, the combustion reaction can be assumed to be complete and therefore the combustion efficiency may be assumed equal to 1. For white phosphorus P_4, the above reaction can also be assumed to be complete[20].

Mixture composition

From Equation (17) and the definitions of the stoichiometric ratios S_{th}, S_{thw} and the mass flow m_F of initial fuel, it can now be derived that the mass flows (kg/s) in the mixture are as follows:

- mass flow of combustion product (pollutant) = $m_c = (1+\chi_A S_{thw}) m_F$:
  - mass flow of unburned fuel $m_{unb} = (1-\chi_A)m_F$
  - mass flow of combustion oxide $m_{oxi} = \chi_A (1 + 0.233 S_{th}) m_F$
  - mass flow of initial nitrogen $m_{N2} = \chi_A (0.767 S_{th}) m_F$
  - mass flow of initial water $m_{wi} = \chi_A (S_{thw} - S_{th}) m_F$

  (19)
- mass flow of moist excess air entrainment = m_{entr}
- total mass flow (kg/s) of the mixture $m_{tot} = m_{entr} + m_c$

[xiv] CORRECT. Former phosphours version erroneously contained 8.01 instead of 1.602, thus underestimated the effect of water on the value of S_{thw}.

Thus the mass fractions η_c, η_{oxi}, η_{N2}, η_{wi}, η_{unb} of the combustion product, oxide, nitrogen, initial water, and unburned fuel in the overall mixture are as follows:

$$\eta_c = \frac{(1+\chi_A S_{thw})m_F}{(1+\chi_A S_{thw})m_F + m_{entr}}, \quad \frac{\eta_{oxi}}{\eta_c} = \frac{\chi_A\,(1+0.233 S_{th})}{1+\chi_A S_{thw}}, \quad \frac{\eta_{N2}}{\eta_c} = \frac{\chi_A\,(0.767\, S_{th})}{1+\chi_A S_{thw}},$$
$$\frac{\eta_{wi}}{\eta_c} = \frac{\chi_A\,(S_{thw}-S_{th})}{1+\chi_A S_{thw}}, \quad \frac{\eta_{unb}}{\eta_c} = \frac{1-\chi_A}{1+\chi_A S_{thw}}$$

The molecular weight of the combustion product M_c and the moist air M_{wa} (kg/kmol) are given by

$$M_c = \left[\frac{\eta_{oxi}/\eta_c}{M_{oxi}} + \frac{\eta_{N2}/\eta_c}{M_{N2}} + \frac{\eta_{wi}/\eta_c}{M_{wi}} + \frac{\eta_{unb}/\eta_c}{M_F}\right]^{-1}, \quad M_{wa} = \left[\frac{\eta_{02}{}^a}{M_{O2}} + \frac{\eta_{N2}{}^a}{M_{N2}} + \frac{\eta_w{}^a}{M_w}\right]^{-1}$$

where the molecular weight M_{oxi} is given by Equation (36) in Appendix A.

Thus the mole fractions y_c, y_{oxi}, y_{N2}, y_{wi}, y_{unb} of the combustion product, oxide, nitrogen, initial water, and unburned fuel in the overall mixture are as follows:

$$y_c = \frac{\eta_c/M_c}{(\eta_c/M_c)+(1-\eta_c)/M_{wa}}, \quad \frac{y_{oxi}}{y_c} = \frac{M_c}{M_{oxi}}\frac{\eta_{oxi}}{\eta_c}, \quad \frac{y_{N2}}{y_c} = \frac{M_c}{M_{N2}}\frac{\eta_{N2}}{\eta_c},$$
$$\frac{y_{wi}}{y_c} = \frac{M_c}{M_w}\frac{\eta_{wi}}{\eta_c}, \quad \frac{y_{unb}}{y_c} = \frac{M_c}{M_{unb}}\frac{\eta_{unb}}{\eta_c}$$

2.5 Thermodynamics

This section aims to provide an approximate description of the pool-fire thermodynamics. Near the source, this approximation is certainly over-simplified given the extreme high temperatures. However near and at the Froude flame height, the temperatures are more moderate and the approximations are envisaged to be of equally order of accuracy than the other simplifying assumptions in the pool-fire model.

Mixture temperature

The final mixture temperature T_m can be obtained by equating the final enthalpy H_{end} to the initial enthalpy H_{start}. The following simplifying assumptions are being made:

- the initial fuel is liquid, with a liquid-pool temperature of T_{pool} ($T_{pool}<T_b$)[xv]
- all water is assumed to be in the vapour phase; this assumption is justifiable given the high fire temperatures likely to arise
- the specific heat C_{pa} of dry air is taken to be constant and equals 1004 J/kg/K
- the specific heats C_{pN2}, C_{pwv} of nitrogen and water-vapour[xvi] are taken to be constant, and equal to 1130, 2160 J/kg/K respectively (values correspond to values at approx. 550C=823K); this may lead to less accurate results for very high temperatures, but is likely to be reasonably accurate at the point of transition with the UDM dispersion model, i.e. at 90% excess air entrainment
- the specific heat C_{poxi} of the combustion oxide is taken to be constant, and its value is taken to be at the fuel boiling temperature T_b; see Appendix B
- the combustion oxide is assumed to be of one phase; an appropriate assumption is expected to be vapour for hydrocarbon fires (CO_2,H_20 oxides) and solid for phosphorus (P_4O_{10} oxide)
- combustion occurs immediately after evaporation; no further combustion occurs
- the unburned fuel is assumed to be liquid[xvii]

[xv] JUSTIFY. For open fires with a mixtures of compounds, several of the compounds may be 'solid' (e.g. wood).

[xvi] CHECK. For a general type of fire the value of 550C may not be always representative, and more direct derivation of specific heats from property database may be more desirable. For hydrocarbons a more typical temperature may be 525K, at which associated specific heats are 1970 J/kg/K for water and 1060 J/kg/K. However these differences are not considered to be significant.

[xvii] JUSTIFY. This assumption was appropriate for phosphorus, but is not generally applicable. Presumable best to normally to assume 100% combustion efficiency, i.e. no presence of liquid.

The initial enthalpy H_{start} (J/s) is the sum of the enthalpy of the initial liquid fuel (flow m_F) and the initial enthalpy of the air (stoichiometric air + exess air; flow m_{tot}-m_F):

$$H_{start} = m_F C_{pL}(T_{pool} - T_r) + (m_{tot} - m_F) C_{pwa}(T_a - T_r) \qquad (20)$$

where $C_{pwa} = [C_{pa}S_{th} + C_{pwv}(S_{thw} - S_{th})]/S_{thw}$ is introduced to be the 'equivalent' specific heat of wet air, and T_r the reference temperature for enthalpy calculation.

The final enthalpy H_{end} (J/s) is the sum of the 'energy required to heat fuel and all air from reference temperature T_r to the liquid boiling temperature T_b', 'the energy needed for the liquid evaporation minus the heat released by the immediate combustion', 'the energy lost because of radiation', and 'the energy needed to heat each of the mixture compounds [see Equation(19)] from the boiling temperature to the final temperature T_m'[xviii]:

$$\begin{aligned} H_{end} \;=\; & m_F C_{pL}(T_b - T_r) \;+\; (m_{tot} - m_F) C_{pwa}(T_b - T_r) \;+ \\ & \chi_a m_F (\Delta H_v - H_{comb}) \;+\; \chi_a \chi_R m_F H_{comb} \;+ \\ & [m_{unb} C_{pL} + m_{oxi} C_{poxi} + m_{N2} C_{pN2} + m_{wi} C_{pwv} + m_{entr} C_{pwa}] (T_m - T_b) \end{aligned} \qquad (21)$$

The temperature is found from Equations (20) and (21) by equating $H_{start} = H_{end}$.

Mixture density

As discussed above, the mixture consists of unburned fuel, combustion oxide, nitrogen, water and dry air. The mixture density ρ_m equals the ratio of the molar mixture weight M_m and the molar mixture volume V_m.

$$\rho_m = \frac{M_m}{V_m} \qquad (22)$$

The molar mixture weight M_m is the ratio of the total mass flow m_{tot} and the total molar flow Q_{tot},

$$M_m = \frac{m_{tot}}{Q_{tot}}, \quad with \quad Q_{tot} = Q_{vap} + Q_{liq} \qquad (23)$$

Here Q_{tot} (nitrogen, water, combustion oxide, unburned fuel, dry air) has been split into the total molar vapour flow Q_{vap} and total non-vapour flow Q_{liq},

$$\begin{aligned} Q_{vap} &= \frac{m_{N2}}{M_{N2}} + \frac{m_w}{M_w} + \frac{m_a}{M_a}, \qquad Q_{liq} = \frac{m_{oxi}}{M_{oxi}} + \frac{m_{unb}}{M_{unb}} \quad \text{(non-vapour comb.oxide)} \\ Q_{vap} &= \frac{m_{N2}}{M_{N2}} + \frac{m_w}{M_w} + \frac{m_{oxi}}{M_{oxi}} + \frac{m_a}{M_a}, \qquad Q_{liq} = \frac{m_{unb}}{M_{unb}} \quad \text{(vapour combustion oxide)} \end{aligned} \qquad (24)$$

where m_w, m_a are the mass flow of total water (initial in combustion product + in excess air) and mass flow of dry air (in excess air), and M_{N2}, M_w, M_a, M_{oxi}, M_{unb} are the molecular weights of nitrogen, water, dry air, combustion oxide and unburned fuel.

The molar mixture volume V_m (m^3/kmole) is obtained from the ideal-gas law for the nitrogen, water and dry air, while ignoring the volumes of non-vapour flow,

$$V_m = \frac{Q_{vap}}{Q_{tot}} \frac{R T_m}{P} \qquad (25)$$

where R is the gas constant (J/kmole/K), and P the pressure (Pa).

Insertion of Equations (23), (25) into (22) leads to the following expression for the mixture density,

[xviii] CORRECT. The older phosphorus version did not include the radiation term for heating the initial water from the boiling temperature to the mixture temperature.

$$\rho_m = \frac{P\, m_{tot}}{R\, T_m\, Q_{vap}} \qquad (26)$$

In the pool fire model POLF the pressure P is assumed to be equal to the atmospheric pressure P_a.

Plume velocity

The plume velocity u_{cld} is derived by equating the total mixture mass flow m_{tot} (kg/s) to the product of the mixture density ρ_m (kg/m^3) and the mixture volume flow $0.25\pi D^2 u_{cld}$:

$$u_{cld} = \frac{m_{tot}}{0.25\, \pi\, D^2\, \rho_m} \qquad (27)$$

3. LINK BETWEEN POOL-FIRE AND RADIATION MODEL

3.1 Flame co-ordinate sets

The pool fire model POLF outputs as input to the radiation model EXPS the flame co-ordinates. The flame length *H*, flame diameter *D* and tilt angle ϕ are used to calculate the three co-ordinates of the flame. The flame co-ordinate sets are assigned as follows (see Figure 4):

$$x_1 = 0.0 \qquad x_2 = H \sin\phi \qquad x_3 = H \sin\phi$$
$$z_1 = z_{pool} \qquad z_2 = H \cos\phi + z_{pool} \qquad z_3 = H \cos\phi + z_{pool}$$
$$r_1 = D/2 \qquad r_2 = D/2 \qquad r_3 = 0.0$$
$$\phi_1 = 0.0 \qquad \phi_2 = 0.0 \qquad \phi_3 = 0.0$$

These equations specify 3 circles, which define the pool fire

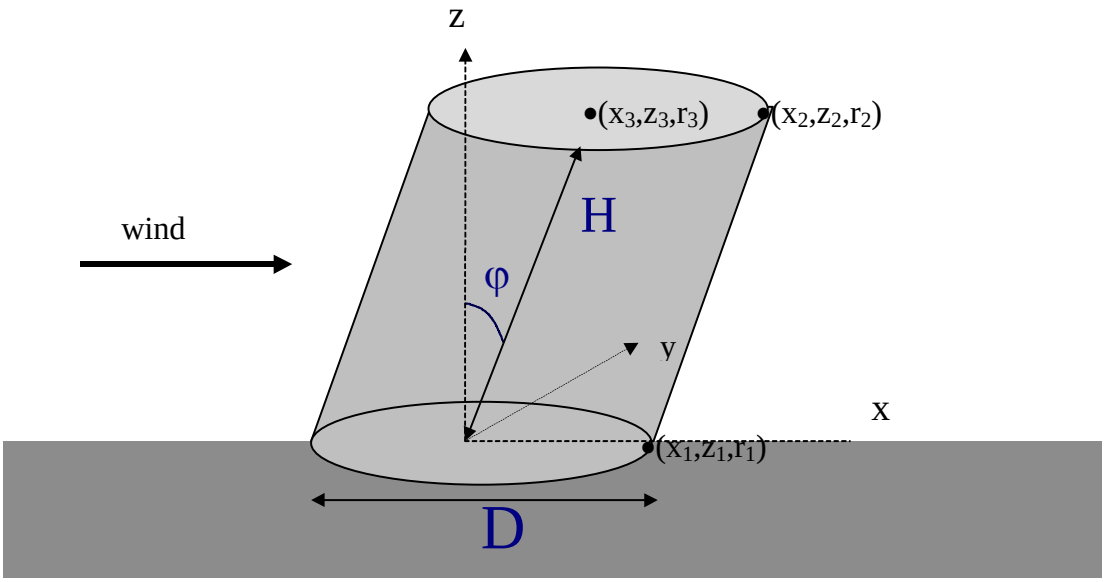

Figure 4. Definition of three sets of flame co-ordinates

3.2 Modification of pool fire location (case of rainout with bund)

This section describes effect of the bund on the location of the centre of the pool in case of linked dispersion (by Phast dispersion model UDM) and POLF pool fire calculations.

In case rainout is outside the bund, there will be no bund effects present in the pool fire modelling and the centre of the pool equals the rainout location.

In case rainout is inside the bund, POLF will apply the correct location of the bund with bund centre at the release point and not at the rainout point for both early and late pool fires. Otherwise it will not affect the calculations of the pool fire model POLF.

When the downwind edge of the pool is at the bund wall, POLF simplistically assume that the tilted cylindrical shape of the pool fire will not be affected by the bund wall, and that there is also no reduction of radiation because of shielding by the bund wall. This assumption would be conservative in case the fire height is not significantly larger than the bund wall height[xix]

[xix] A warning could be considered to be added in case the fire height less than the bund wall height

Evaluation of location of downwind distance of centre of pool fire

If the UDM droplet hits the bund wall, UDM rainout is assumed to occur at the bund wall. In this case the downwind edge of the early and late pool fires is taken equal to the downwind edge of the bund wall; see Figure 5a.

If droplet rains out inside the bund, the centre of the pool fire is at the rainout point (downwind distance) x_{ro} if the pool fire does not hit the downwind edge of the bund wall; see Figure 5b. However when it hits the bund wall, the downwind edge of the pool fire is at the downwind edge of the bund wall; see Figure 5a.

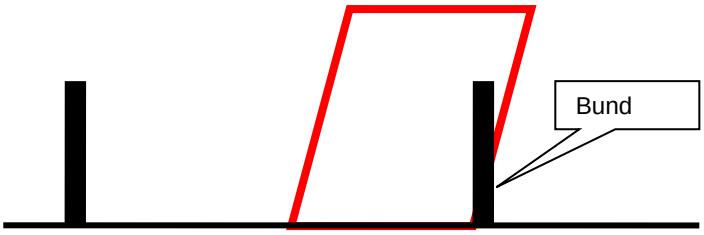

(a) Droplet hits bund; or in case of rainout inside bund, pool fire edge reaches bund wall

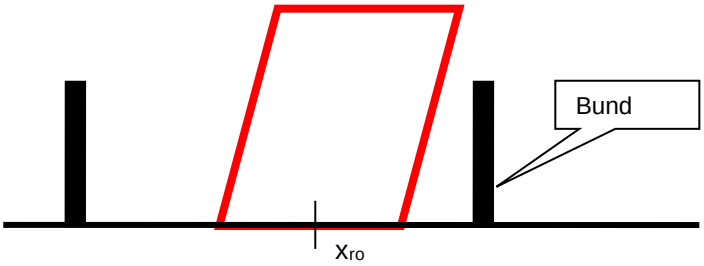

(b) Case of rainout inside bund, with pool fire edge not reaching bund wall

Figure 5. Location of pool fire in case of rainout inside bund

Thus the downwind distance x_{pool} of the centre of the pool fire from the release location (=centre of the bund, in case of presence of bund) is calculated as follows:

$$\begin{aligned} x_{pool} &= x_{ro} \text{ , rainout outside bund} \\ x_{pool} &= R_{bund} - \frac{D}{2} \text{ , drop hits bund } (x_{ro} = R_{bund}) \\ x_{pool} &= \max\left\{0, \min\left[x_{ro}, R_{bund} - \frac{D}{2}\right]\right\} \text{ , rainout inside bund } (x_{ro} < R_{bund}) \end{aligned} \qquad (28)$$

3.3 Radiation calculations in radiation model

The radiation intensity I is derived by means of integration of the surface emissive power E_f [see Equation (9)] along the flame surface,

$$I = E_f \, F \qquad (29)$$

with the view-factor F, including the effects of atmospheric absorption τ, given by

$$F_{A_1 \to dA_2} = \iint_{A_1} \frac{\tau \cos(\beta_1) \cos(\beta_2)}{\pi \ \mathrm{r}^2} dA_1 \qquad (30)$$

The integration is carried out numerically over the flame surface A_1 to the constraint that only contributions for which $\cos(\beta_1)$ and $\cos(\beta_2)$ are positive are included[xx]. The meaning of the variables in Equation (30) is illustrated by Figure 6: r is the distance between the fire element dA_1 and the receiving element dA_2, β_1 is the angle between the normal to dA_1 and the line $dA_1 \to dA_2$, and β_2 is the angle between the normal to dA_2 and the line $dA_1 \to dA_2$.

The atmospheric transmissivity τ is taken from Wayne[21] in terms of the variables $X(H_2O)$ and $X(CO_2)$ representing the amount of atmospheric water vapour and atmospheric carbon dioxide in the path between the radiator and the receptor.

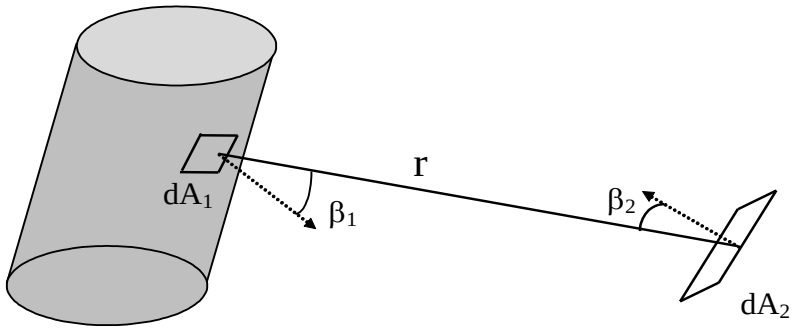

Figure 6. Radiation from fire element dA_1 received by element dA_2

See the theory description of the radiation model EXPS fur further details.[22]

[xx] JUSTIFY. Mudan states that integration is to be carried out over the entire surface of the flame. What is correct?

4. VERIFICATION AND VALIDATION

This chapter discusses the validation and verification of the pool fire model described above (POLF) in conjunction with the DNV radiation model (EXPS). This supersedes validation earlier description in the PHAST 4.2 release notes[7].

Predictions from the model are validated by comparing against field measurements reported by Johnson[17], Nedelka et al[23] for LNG and Lois and Swithenback[24] for n-Hexane pool flames. For the validation and verification exercises, LNG is assumed to be composed of pure methane[17, 23]. In addition, the Johnson correlation is employed for flame tilt angle calculations. The validation of the radiation model (EXPS) (based on the POLF simulated flame characteristics) is conducted by comparing its predicted incident radiant flux at specified observer locations and orientations with measured data.

For the verification exercise, the predictions from the POLF and EXPS models are compared with simulated data for LNG (methane) pool flames reported by Johnson[17].

4.1 Verification and validation of the POLF-EXPS models against data reported by Johnson, 1992

The following presents and discusses the results of the verification and validation of the POLF and EXPS models against field data and simulated results reported by Johnson [17].

Three tests that relate to 1.8, 6.1, and 10.6m diameter LNG pool flames (i.e. Field Trials 1, 6 and 7 respectively) were reported. The tests were carried out in shallow bunds with floors of thermally insulated concrete so as to minimise the heat transfer to the pool from the substrate. Table 1 contains a summary of pool and ambient data for each test, while

Table 2 lists the Cartesian coordinates and orientations of different observer (radiometer) positions at which radiation intensities were measured.

Table 1 Summary of pool and ambient data for field trials 1, 6 and 7 [17]

	Field Trial -1	Field Trial-6	Field Trial-7
Pool diameter [m]	1.8	6.1	10.6
Air Temperature [K]	283.15 (assumed)[xxi]	280.15	282.45
Air pressure [bar]	1.01325 (assumed)[xxi]	0.943	0.943
Relative Humidity (%) [-]	70 (assumed) [xxi]	83	87
Wind Speed [m/s]	2.4	6.6	4.0
Wind direction, clockwise from North	270	250	90

The x, y and z axes of the coordinate system correspond to the wind direction, the horizontal line perpendicular to the wind direction which passes through the bund centre and the vertical directions respectively. The origin of the coordinate system is located at the bund centre. The angles ξ and γ refer, respectively, to the angle of inclination of the observer from the horizontal, and the horizontal orientation of the normal to the radiometer face from the negative x direction.

[xxi] NOTE: Johnson does not report values for ambient pressure, temperature and relative humidity for Field Trial-1. The author however points out that these variables are of little importance to incident radiation calculations as atmospheric pathlengths from specified receiver positions during the test are less than 10m.

Table 2 **Observer (radiometer) position and orientation with respect to bund centre for Field Trials 1, 6 and 7**

Field Trial 1				
x [m]	y [m]	z [m]	ξ [degrees]	γ [degrees]
6.20	1.09	1.0	0	-10.0
5.92	-2.15	1.0	0	20.0
4.83	4.05	1.0	0	-40.0
2.15	5.92	1.0	0	-70.0
-1.09	6.20	1.0	0	0.0
Field Trial 6				
x [m]	y [m]	z [m]	ξ [degrees]	γ [degrees]
9.58	26.31	1.07	0	-70.0
11.29	31.01	1.07	0	-70.0
32.50	5.73	1.07	0	-10.0
41.36	7.29	1.07	0	-10.0
23.49	-8.55	1.07	0	20.0
31.01	-11.29	1.07	0	20.0
35.71	-13.00	1.07	0	20.0
39.47	-14.36	1.07	0	20.0
-14.10	5.13	1.07	0	-160.0
-16.91	6.16	1.07	0	-160.0
-23.49	8.55	1.07	0	-160.0
-16.07	19.15	1.07	0	-130.0
-21.20	25.28	1.07	0	-130.0
Field Trial 7				
x [m]	y [m]	z [m]	ξ [degrees]	γ [degrees]
0.00	-38.00	1.25	0	90.0
0.00	-48.00	1.25	0	90.0
0.00	-56.00	1.25	0	90.0
-27.00	-46.76	1.25	0	120.0
-28.58	-16.50	1.25	0	150.0
-36.37	-21.00	1.25	0	150.0
-43.30	-25.00	1.25	0	150.0
-33.00	0.00	1.25	0	180.0
-38.00	0.00	1.25	0	180.0
-50.00	0.00	1.25	0	180.0
48.00	0.00	1.25	0	0.0
56.00	0.00	1.25	0	0.0
63.50	0.00	1.25	0	0.0

Table 3 compares measured pool fire characteristics (where available) for trials 1, 6 and 7 with simulated results using the POLF and Johnson[17] models.

Table 3 Comparison of measured pool fire characteristics with simulated results using the POLF and Johnson[17] pool fire models

Field Trial 1			
Flame parameters	**Measured data**	**Johnson Model**	**POLF**
Flame length [m]	-	3.31	3.31
Flame tilt [degrees]	47.5 (±6.5)	48.6	48.61
Mass burning rate [$kgm^{-2}s^{-1}$]	-	0.03	0.03
Surface emissive power [kWm^{-2}]	-	56.1	51.5
Field Trial 6			
Flame parameters	**Measured data**	**Johnson Model**	**POLF**
Flame length [m]	-	14.3	14.35
Flame tilt [degrees]	57.4 (±6.6)	58.2	58.24
Mass burning rate [$kgm^{-2}s^{-1}$]	0.085	0.079	0.080
Surface emissive power [kWm^{-2}]	-	122.6	130.88
Field Trial 7			
Flame parameters	**Measured data**	**Johnson Model**	**POLF**
Flame length [m]	-	25.3	25.44
Flame tilt [degrees]	42.2 (±7.1)	47.1	47.14
Mass burning rate [$kgm^{-2}s^{-1}$]	0.105-0.107	0.108	0.108
Surface emissive power [kWm^{-2}]	-	158.1	174.25

From Table 3 the following can be observed:

- There is close semblance in simulated results obtained from the POLF and Johnson pool fire models for flame length tilt and mass burning rate.
- Within limits of uncertainty, simulated pool flame characteristics based on the POLF and Johnson pool fire models show good agreement with available field data.
- There is less agreement between simulated flame surface emissive power (SEP) obtained from POLF and the Johnson pool fire model. Likely reasons for these differences are:
    - The use of different values of E_m and L_s in equation (9) in the POLF and Johnson pool fire models
    - The algorithm employed in the Johnson model for the calculation of the overall flame SEP differs from the POLF algorithm. The former accounts for the effect of downwind flame drag.

Figure 7 shows the variation of predicted incident radiation [kW/m^2] with measured data for field trials 1, 6 and 7 based on the flame characteristics predicted by the POLF-EXPS models. The reported values of incident radiation predicted by the Johnson pool flame and radiation model at each observer location are also presented. Incident radiations corresponding to 0, ±15 and ±40% from measured data are represented by linear plots on Figure 7.

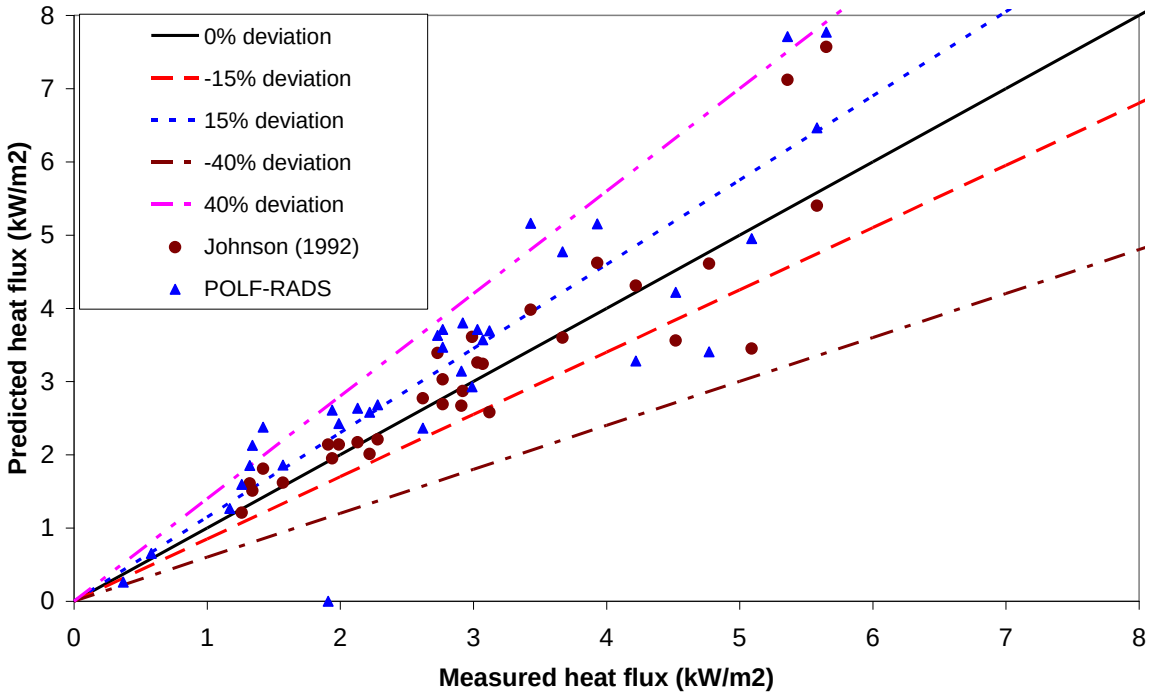

Figure 7 **Variation of predicted against measured incident radiation at different observer positions and orientations using the POLF-EXPS and the Johnson pool fire + radiation models.**

From Figure 7, the following observations are made:

- Within limits of uncertainty in measurements, good agreement is observed between the predicted and measured incident radiation for the POLF-EXPS model. In addition, there is good semblance in simulated results from the POLF-EXPS and Johnson pool fire plus radiation model. Simulated results generally lie within ±40% of measured data.
- The POLF-EXPS model generally predicts higher (more conservative) incident radiation when compared with simulated results from the Johnson pool fire plus radiation model. The observed differences in simulated results obtained from both models are primarily due to differences in their simulated flame SEPs. For all test cases, the higher the flame SEPs predicted by POLF when compared with the Johnson pool fire model, the higher the corresponding incident radiation predicted by each model's radiation model.
- On average, the percentage absolute deviation from measured data of the POLF-EXPS and Johnson-1992 simulated results are ca 28.8% and 12% respectively.

4.2 Validation of the POLF-EXPS models against data reported by Nedelka et al. (1990) and Lois and Swithenback

The following presents and discusses the results of the validation of the POLF-EXPS models against measured radiation intensities around a 35m diameter LNG (methane) and a 6m diameter n-Hexane pool fire reported by Nedelka et al[23] and Lois and Swithenback[24] respectively. Table 4 contains a summary of pool and ambient data for each test, while Table 5 lists the Cartesian coordinates of different observer (radiometer) positions at which radiation intensities were measured for the n-Hexane pool fire.

The observer in each of the n-Hexane pool fire radiation measurements was oriented to receive maximum radiation intensity. Ambient conditions and observer height during the n-Hexane pool fire tests were not reported, as such, the observer is assumed to be at ground level and weather data quoted in Table 4 for the n-Hexane test are assumed. The x, y and z axes and the angles ξ and γ are as previously defined (see section 4.1).

For the LNG test, the pool flame was contained in a shallow 35m diameter bund with floors of thermally insulated concrete. Radiation intensities were measured with radiometers aimed horizontally towards a point 1m above the bund centre[23]. The results of the radiation measurements were presented in terms of 2.5, 5 and 7.5kW/m^2 radiation contours measured with reference to the bund centre. Corresponding radiation contours are estimated by the POLF-EXPS model as radiation ellipses around the pool flame.

Table 4 Summary of pool and ambient data for LNG and n-Hexane pool flames reported by Nedelka et al[23] and Lois and Swithenback[24] respectively

	LNG-pool fire	n-Hexane pool fire
Pool diameter [m]	35	6
Air Temperature [K]	294.15	288
Air pressure [bar]	1.015	1.01325
Relative Humidity (%) [-]	54	70
Wind Speed [m/s]	9.6	0.1
Wind direction, clockwise from North	180	270

Table 5 Observer (radiometer) position and orientation with respect to pool centre for the n-Hexane pool fire test reported by Lois and Swithenback[24]

x [m]	y [m]	z [m]	ξ [degrees]	γ [degrees]
33.6	0	0	-	-
46.7	0	0	-	-
72.6	0	0	-	-

Table 6 compares measured radiation intensities at specified observer locations with simulated results using the POLF-EXPS model. From Table 6 simulated results are seen to compare well with measured data. On average, the percentage absolute deviation of simulated results using the POLF-EXPS model from measured data is ca 16.7%.

Table 6 Comparison of measured radiation intensities with simulated results using the POLF-EXPS model for the n-Hexane pool fire test reported by Lois and Swithenback[24]

x [m]	Observed [kW/m^2]	POLF-EXPS [kW/m^2]
33.6	1.17	1.27
46.7	0.58	0.65
72.6	0.37	0.26

Figure 8 compares the measured and POLF-EXPS simulated 2.5, 5 and 7.5kW/m^2 radiation contours around the LNG pool flame.

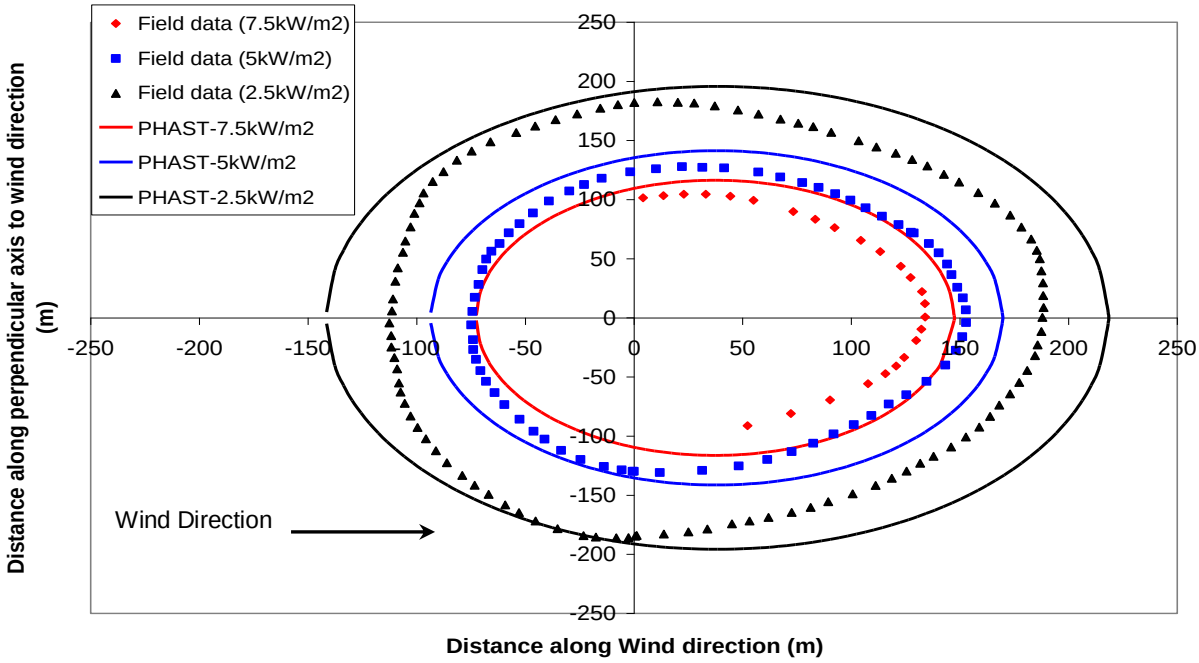

Figure 8 **Comparison of measured versus predicted radiation contours using the POLF-EXPS model (LNG pool flame; Montoir experiments reported by Nedelka et al.)**

From Figure 8, the following observations can be made:

- Simulated radiation contours by the POLF-EXPS model compare well with measured data and generally lie within +30% of observer distances.
- The POLF-EXPS model predicts wider (more conservative) radiation contours around the pool flame when compared with measured data.
- Crosswind estimates of radiation intensities by the POLF-EXPS model are generally closer to measured data than downwind estimates.

In all, from the validation exercises conducted above, the POLF-EXPS model is seen to perform reasonably well when compared with logged pool fire and radiation intensity data. Modelling results obtained from the simulation of radiation intensities/contours around 1.8, 6.1, 10.6 and 35m diameter LNG pool flames and a 6m diameter n-Hexane pool flame, generally lie within ±40% of measured data.

4.3 Verification of the two-zone pool fire model (POLF-TwoZone)

The sensitivity of the two-zone pool fire model to pool material, pool diameter and wind speed are discussed below. The predicted luminous flame length ratio, i.e. flame length of the luminous base zone to the total flame length, for three pool files at two wind speeds, is shown in Figure 9. Table 7 contains a summary of the pool and ambient data assumed to apply in each case. The studied pool fires are 20m in diameter and differ in material make-up, i.e. CH ratio.

Table 7 Summary of pool and ambient data for the assessment

	N-Pentane pool fire	n-Heptane pool fire	N-Nonane pool fire
Pool diameter [m]	20	20	20
Air Temperature [K]	270	270	270
Air pressure [bar]	1.01325	1.01325	1.01325
Relative Humidity (%) [-]	70	70	70
Wind Speed [m/s]	1	1	1

The following observations could be made on relative size of the two zones, i.e.:

- Luminous flame length ratio decreases with pool diameter. So large pool fires would be more smoky than smaller diameter fires at the same conditions.
- Luminous flame length ratio decreases for heavier hydrocarbons. Pool fires of heavier hydrocarbons are more smoky.
- Luminous flame length ratio increases with wind speed. Smoke is dispersed more quickly by strong winds.

Figure 10 compares the predicted radiation along a transect in the downwind direction between the uniform SEP (i.e. POLF) and the two-zone (i.e. POLF-TwoZone) pool fire models for the heptane pool fire scenario detailed in Table 7. The following observations could be made:

- The two-zone pool fire model simulates more conservative predictions in the near field of the fire where the luminous base zone has a strong effect.
- The two modelling approaches give similar predictions in the far field.
- The above trends in model predictions are expected and verify/confirm the merits of the two-zone model.

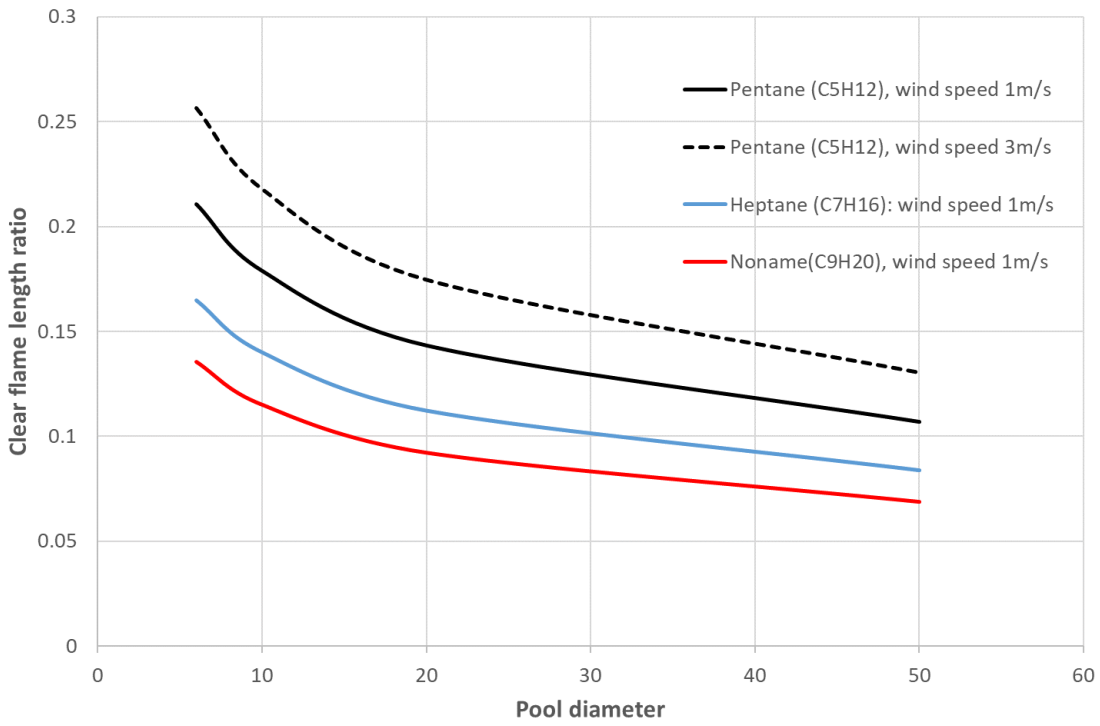

Figure 9 Sensitivity of Clear flame length ratios of two-zone pool fires to materials and wind speeds

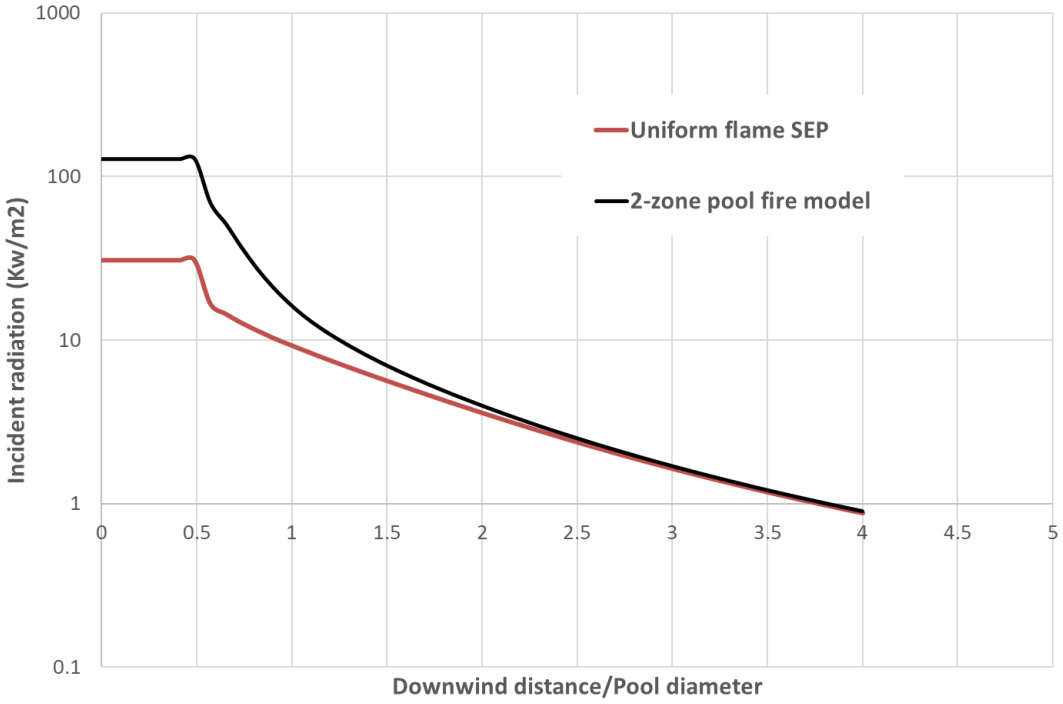

Figure 10 Comparing the predicted radiation assuming uniform SEP (i.e. POLF) and two zones (i.e. POLF-TwoZone)

5. SENSITIVITY ANALYSIS[xxii]

Sensitivity analysis for pool fire model

The pool fire model described in the previous section has been tested extensively. A detailed sensitivity analysis has been carried out to analyse the results and to ensure the correctness of the program. Appendix D includes details of the selected basecase values and the parameter variations.

A burning propane pool is selected as the basecase with a wind speed of 0.5 m/s and a liquid spill rate of 4 kg/s. The input data that have been varied include all input variables:

- ambient data: speed, temperature, pressure, humidity
- fuel data: material type, combustion efficiency, specific heat of combustion oxide, phase for combustion oxide
- pool data: temperature, spill rate, elevation, on land or water, bund diameter
- parameters defined special calculations with one or more output data specified by the user (flame length, flame angle, flame diameter, burn rate, surface emissive power, radiative fraction).

To include examples figures for variation of spill rate, variation of wind speed, and variation of material

Example for combined pool fire and dispersion calculations (to add)

[xxii] IMPROVE. To add example results

6. FUTURE DEVELOPMENTS

The following future developments are proposed.

1. More accurate modelling of thermodynamics:
   - Accurate modelling of multi-compound thermodynamics in the UDM including the possibility of solid compounds (e.g. smoke particles).
   - The evaluation of the specific heat and phase of combustion oxides may be automated via the property system (e.g via specifying CAS numbers and reaction moles for each component in combustion oxide).
   - More accurate description of the pool-fire thermodynamics, and incomplete combustion (e.g. presence of both carbon monoxide and carbon dioxide).
   - Possible improvement of formulation for less than 100% combustion efficiency. Equations (10) and (9) may not be appropriate (and perhaps also others) if the combustion efficiency $\chi_a < 1$.
   - Inclusion of reactions in the dispersion model[8,9] where accurate kinetic rate constants are needed. The reaction rate constant may be varied to compare the difference between zero, slow, fast and complete reaction. Further improvements could include formation of phosphoric acids and phosphorus oxides, temperature-dependency of reaction rate, reactions for other compounds (ammonium, sulphide trioxide, phosphine, phosphorus chlorides,....), incomplete reactions (equilibrium constants), and multi-compound rainout (i.e. both reactants and products).
2. More accurate modelling of non-zero wind-speed effects may involve:
   - An alternative more appropriate flame-length formula[25].
   - The excess-air entrainment formulation by Delichatsios[10] is based on zero wind-speed experimental data, and needs extension for non-zero wind speeds.
   - An elliptical cross section (larger diameter in the downwind direction) for the fire rather than a circular one will be more accurate (wind-speed drag)[2].
3. The excess-air entrainment formulation may need further extension for small stoichiometric air to fuel ratios (near to 1).
4. Further validation against experimental data is desirable (air entrainment, fire dimensions, radiation, smoke generation).
5. The model now provides a transition from a pool-fire model to smoke dispersion. An additional model may be developed for a link between a turbulent jet flame and smoke dispersion. Herewith use may be made of the formulation of Delichatsios for small Froude numbers.
6. To further address several of the footnotes included in this report (DOC,JUSTIFY,CHECK,IMPROVE).

APPENDICES

Appendix A Evaluation of stoichiometric ratio for fuel combustion reaction

General derivation from MDE flammable properties

The theoretical stoichiometric mass ratio S_{th} is defined to be the mass ratio of dry air needed to the mass of fuel needed in case of complete combustion,

$$S_{th} = \frac{mass\ of\ dry\ air\ needed\ for\ complete\ combustion}{mass\ of\ fuel} \quad (31)$$

The MDE flammable material properties A_t, C_t are defined as

$$A_t = \frac{moles\ of\ fuel + moles\ of\ air}{moles\ of\ combustion\ products} \quad (32)$$

$$C_t = \frac{moles\ of\ fuel}{moles\ of\ fuel + moles\ of\ air} \quad (33)$$

The air consists of 79 mole % nitrogen (N_2) and 21 mole % oxygen (O_2). Assuming complete combustion of the fuel into combustion oxide, the reaction is as follows:

$$C_t\{fuel\} + [1-C_t]\{0.21\,O_2 + 0.79\,N_2\} \rightarrow [A_t^{-1} - 0.79(1-C_t)]\{comb.\,oxide\} + [1-C_t]\{0.79\,N_2\} \quad (34)$$

Thus C_t mole of fuel reacts with $[1-C_t]$ moles of air, to form as combustion products $[A_t^{-1} - 0.79(1-C_t)]$ mole of combustion oxide and $0.79[1-C_t]$ moles of nitrogen N_2.

The molecular weight of dry air is $M_{air} = 0.79\ M_{N2} + 0.21\ M_{02}$, with the molar masses $M_{02} = 32$ kg/kmol, $M_{N2} = 28$ kg/kmol. Thus following the above reaction (34) the stoichiometric ratio S_{th} is given by

$$S_{th} = \frac{1-C_t}{C_t}\frac{M_{air}}{M_{fuel}} \quad (35)$$

where M_{fuel} is the molecular weight of the fuel.

From the above reaction (34) it also follows that the molecular weight M_{oxide} of the combustion oxides is given by

$$M_{oxide} = \frac{C_t M_{fuel} + [1-C_t]0.21 M_{O_2}}{A_t^{-1} - 0.79\,[1-C_t]} \quad (36)$$

Stoichiometry of combustion for hydrocarbon (C_nH_{2n+2})

Assuming complete combustion of the hydrocarbon C_nH_{2n+2} into carbon dioxide, the combustion reaction is as follows:

$$C_nH_{2n+2} + 0.5(3n+1)\,[O_2 + (0.79/0.21)N_2] \rightarrow n\,CO_2 + (n+1)\,H_2O + 0.5(3n+1)\,(0.79/0.21)N_2$$

The theoretical stoichiometric mass ratio S_{th} is defined to be the mass ratio of dry air needed to the mass of fuel needed in case of complete combustion. Using the molar masses $M_{02} = 32$, $M_{N2} = 28$, $M_{CnH2n+2} = (14n+2)$ kg/kmol, it follows that:

$$S_{th} = 0.5(3n+1)\,[M_{O2} + (0.79/0.21)M_{N2}] / M_{C14H30} = 103[n+1/3]/[7n+1]$$

This leads to S_{th} = 14.9 for kerosene (n=14) and S_{th} = 15.6 for propane (n=3). The value for kerosene corresponds to the value S_{th} = 15 quoted by Delichatsios.

$$A_t = \frac{moles\ of\ \ fuel + moles\ of\ air}{moles\ of\ combustion\ products} = \frac{1+0.5(3n+1)[1+(0.79/0.21)]}{2n+1+0.5(3n+1)(0.79/0.21)}$$

$$C_t = \frac{moles\ of\ \ fuel}{moles\ of\ \ fuel + moles\ of\ air} = \frac{1}{1+0.5(3n+1)[1+(0.79/0.21)]}$$

Note that C_t equals the stoichiometric concentration of combustion in air (mole fraction of fuel). The data as calculated above were confirmed to agree with the material database for the case of $C_{14}H_{30}$ (kerosene).

Note that complete combustion is assumed in POLF. In case of incomplete combustion a lower value of S_{th} is applied. For example, assuming incomplete combustion of kerosene into carbon monoxide, the reaction is as follows:

$$C_{14}H_{30} + 14.5\ [O_2 + (0.79/0.21)N_2] \rightarrow 14\ CO + 15\ H_2O + 14.5(0.79/0.21)N_2$$

and

$$S_{th} = 14.5[M_{O2} + (0.79/0.21)M_{N2}] / M_{C14H30} = 10.04$$

Stoichiometry of combustion for white phosphorus (P_4)

P_4 reacts with dry air as follows

$$P_4 + 5\ [O_2 + (0.79/0.21)N_2] \rightarrow P_4O_{10} + 5\ (0.79/0.21)N_2$$

Thus using M_{P4} = 124 kg/kmol,

$$S_{th} = 5\ [M_{O2} + (0.79/0.21)M_{N2}] / M_{P4} = 5.54$$

$$A_t = \frac{moles\ of\ \ fuel + moles\ of\ air}{moles\ of\ combustion\ products} = \frac{1+5[1+(0.79/0.21)]}{1+5(0.79/0.21)} = 1.25$$

$$C_t = \frac{moles\ of\ \ fuel}{moles\ of\ \ fuel + moles\ of\ air} = \frac{1}{1+5(0.79/0.21)]} = 0.0403$$

Appendix B Evaluation of specific heat of combustion oxide

The mass fraction of the combustion oxide is obtained using the model of Delichatsios. Thermodynamics evaluation requires the evaluation of the specific heat of the combustion oxide.

In case of reaction of phosphorus with air, the combustion oxide is purely P_4O_{10}, and no water forms during the reaction. Thus the specific heat of the combustion oxide can be directly obtained from the specific heat of P_4O_{10}.

In case of reaction of hydrocarbon C_nH_{2n+2} with air (complete combustion), the combustion oxide consists of carbon dioxide CO_2 [mole fraction n/(2n+1)] and water H_2O [mole fraction (n+1)/ (2n+1)]. Thus the specific heat of the combustion oxide should correspond to this mixture of CO_2 and H_2O. The mass fraction η_{CO2}^{oxi} of CO_2 in the combustion oxide equals:

$$\eta_{CO2}^{\ oxi} = \frac{n\,M_{CO2}}{n\,M_{CO2} + (n+1)M_w} \qquad (37)$$

where the CO_2 molecular weight M_{CO2} = 44 kg/kmole, and the water molecular weight M_w = 18 kg/kmole. Thus the specific heat of the combustion oxide equals:

$$C_p^{\ oxi} = \eta_{CO2}^{\ oxi}\, C_p^{\ CO2} + (1-\eta_{CO2}^{\ oxi})C_p^{\ w} \qquad (38)$$

The above calculation is now applied for the case of kerosene (n=14). The mass fraction of CO_2 in the combustion oxide is found from Equation (37): η_{CO2}^{oxi} = 0.695. Between the ambient temperature of 293K and the kerosene boiling temperature of 526.7 K the specific vapour heat for CO_2 varies between 840 and 1030 J/kg/K and that of water between 1860 and 1970 J/kg/K. Using the values at the boiling temperature T_b= 526.7 K [C_p^{CO2} = 1030 J/kg/K, C_p^{w} = 1970 J/kg/K], the specific heat of the combustion oxide at T_b is found from Equation (38): C_p^{oxi} = 1316.7 J/kg/K.

Appendix C Spreadsheets for calculation of properties of combustion product

Two spreadsheets have been developed for calculation of the properties of the combustion product.

The first spreadsheet is developed to calculate the properties of the combustion product in case of a hydrocarbon; see Appendix A, Appendix B and Section 2.3 for details of the calculations. A sample copy of this spreadsheet is included below. This spreadsheet allows for data to be calculated for a range of hydrocarbons.

The second spreadsheet is developed to calculate the properties of the combustion product in case of a more general combustion reaction:

$$n_F F + n_{O2} O_2 + n_{N2} N_2 \rightarrow n_{N2} N_2 + \sum_{i=1}^{n} n_i P_i \quad (39)$$

Thus n_F moles of fuel F react with n_{O2} moles of oxygen O_2 from the air to form a combustion oxide consisting of n reaction products $P_1,\ldots P_n$ (number of moles n_i, molecular weight M_i, i=1,…n). After the combustion reaction, n_{N2} moles of nitrogen N_2 [$n_{N2} = (0.79/0.21)\, n_{O2}$] remain from the stochiometric air. Thus the entire combustion product consists of the combustion oxide and the nitrogen remaining from the stochiometric air.

In the spreadsheet the user needs to define the fuel name, fuel molecular weight, and the reaction (number of moles n_F, n_{O2}, and $n_1,\ldots n_n$, with n=10 adopted in the spreadheet). In case the user wishes to specify a product not already present in the spreadsheet, he needs to specify the name, molecular weight and specific vapour heat for the product.

The calculation of the properties is carried out in analogy to the hydrocarbon properties. The molecular weight of the combustion oxide M_{oxi}, and the mass fraction η_i^{oxi} (i=1,…n) in the combustion oxide are calculated as:

$$M_{oxi} = \frac{\sum_{i=1}^{n} n_i M_i}{\sum_{i=1}^{n} n_i}, \qquad \eta_i^{oxi} = \frac{n_i M_i}{\sum_{i=1}^{n} n_i M_i} \quad (40)$$

The molecular weight of the combustion oxide M_c, and the mass fraction η_i^c and mole fraction y_c^i of product P_i (i=1,… n) in the combustion product are given by

$$M_c = \frac{(1-\chi_a) n_F M_F + \chi_a \left[n_{N2} M_{N2} + \sum_{i=1}^{n} n_i M_i \right]}{(1-\chi_a) n_F + \chi_a \left[n_{N2} + \sum_{i=1}^{n} n_i \right]} \quad (41)$$

$$\eta_i^c = \frac{\chi_a n_i M_i}{(1-\chi_a) n_F M_F + \chi_a \left[n_{N2} M_{N2} + \sum_{i=1}^{n} n_i M_i \right]}, \quad y_i^c = \eta_i^c \frac{M_c}{M_i} \quad (42)$$

The combustion reaction factors A_t, C_t and the stochiometric ratio S_{th} for Equation (39) are set using Equations (32),(33),(35). The specific heat of the combustion oxide C_p^{oxi} is set from the mass fractions η_i^c and the specific vapour heat C_p^i (i=1,…10) of the products as

$$C_p^{oxi} = \sum_{i=1}^{n} \eta_i^{oxi} C_p^i \quad (43)$$

Spreadsheet to set properties of combustion product for hydrocarbon fire

- water in stochiometric air is ignored; air consists of 0.79 mole fraction N2 and 0.21 mole fraction O2
- total combustion product consists of unburned fuel, N2 (from stochiometric air) and H20,CO2 (='combustion oxide')
- user must input yellow cells only, and should not change other cells

I/O VARIABLE	RUN1	RUN2	RUN3	RUN4	RUN5	RUN6	Ref. Theory
Input data:							
name of hydrocarbon (CnH2n+2)	methane	ethane	propane	hexane	octane	kerosene	
n	1	2	3	6	8	14	
combustion efficiency (= mass fraction of fuel that is burned)	1	1	1	1	1	1	
Input parameters (don't normally change):							
- specific heat of H20 at 525K (J/kg/K)	1970	1970	1970	1970	1970	1970	App. B
- specific heat of CO2 at 525K (J/kg/K)	1030	1030	1030	1030	1030	1030	App. B
Output data:							
Dry stoichiometric ratio	17.1667	16.0222	15.6061	15.1705	15.0585	14.9125	App. A
Combustion reaction factors:							
- AT	1	0.97248	0.96125	0.94871	0.94533	0.94085	App. A
- CT	0.09502	0.0566	0.04031	0.02163	0.01652	0.00967	App. A
Mass fractions in combustion product:							
- combustion oxide	0.27522	0.27806	0.27919	0.28043	0.28076	0.2812	Sect. 2.3
* CO2	0.15137	0.17232	0.18065	0.18983	0.19227	0.19551	Sect. 2.3
* H20 (assume dry air)	0.12385	0.10574	0.09854	0.0906	0.08849	0.08569	Sect. 2.3
- N2	0.72478	0.72194	0.72081	0.71957	0.71924	0.7188	Sect. 2.3
- unburned fuel	0	0	0	0	0	0	Sect. 2.3
Molecular weights (kg/kmol):							
- fuel CnH2n+2	16	30	44	86	114	198	App. A
- combustion oxide	26.6667	28.4	29.1429	30	30.2353	30.5517	App. A
- combustion product (assume dry air)	27.6199	28.1101	28.31	28.5334	28.5935	28.6734	Sect. 2.3
Mole fractions in combustion product:							
- combustion oxide	0.28506	0.27522	0.27121	0.26672	0.26552	0.26391	Sect. 2.3
* CO2	0.09502	0.11009	0.11623	0.1231	0.12495	0.12741	App. B
* H20 (assume dry air)	0.19004	0.16513	0.15498	0.14362	0.14057	0.13651	App. B
- N2	0.71494	0.72478	0.72879	0.73328	0.73448	0.73609	Sect. 2.3
- unburned fuel	0	0	0	0	0	0	Sect. 2.3
Specific heat of combustion oxide at 525K (J/kg/K)	1453	1387.46	1361.76	1333.69	1326.26	1316.46	App. B

Spreadsheet to set properties of combustion product for fire (general combustion reaction)

- water in stochiometric air is ignored; air consists of 0.79 mole fraction N2 and 0.21 mole fraction O2
- total combustion product consists of unburned fuel, N2 (from stochiometric air) and products 1-10 (='combustion oxide')
- user must input yellow cells only, and should not change other cells

combustion efficiency (= mass fraction of fuel that is burned)	1						
Definition of combustion reactants/products:	name	mole weight (kg/kmol)	specific heat at 525K (J/kg/K)	#moles in reaction	mass fraction in combustion oxide	mass fraction in combustion product	mole fraction in combustion product
- fuel	propane	44		1		0	0
- stoichiometric air - O2	O2	32	1004	5			
- stoichiometric air - N2	N2	28	1130	18.8095		0.72080292	0.728782288
- product 1	CO2	44	1030	3	0.647058824	0.180656934	0.116236162
- product 2	H20	18	1970	4	0.352941176	0.098540146	0.15498155
- product 3	CO	28	1070	0	0	0	0
- product 4	N02	46	950	0	0	0	0
- product 5	NO	30	1165	0	0	0	0
- product 6	SO2	64	740	0	0	0	0
- product 7	HCL	36.46	800	0	0	0	0
- product 8	HCL	36.46	800	0	0	0	0
- product 9	N2	28	1060	0	0	0	0
- product 10	P4010	284	500	0	0	0	0
TOTAL					1	1	1

produced combustion oxide (kg / kmole of burned fuel)	204
produced total combustion product (kg / kmole of total fuel)	730.667
molecular weight of combustion oxide (kg/kmol)	29.1429
molecular weight of combustion product (kg/kmol)	28.31
specific heat of combustion oxide at 525K (J/kg/K)	1361.76
Dry stoichiometric ratio	15.6061
Combustion reaction factors:	
- AT	0.96125
- CT	0.04031

Appendix D Sensitivity analysis: base-case input data and parameter variations

Inputs		DNV POOL FIRE MODEL POLF_2 [POLF extension for RIVM - user-specified burn rate]								
Input	Description	Units	BASECASE	VAR2	VAR3	VAR4	VAR5	VAR6	VAR7	NOTES
Index										
Ambient Data										
1	Wind Speed	m s-1	0.5	0	5	10	15	65		
2	Temperature	K	300	250	275	325				
3	Pressure	N m-2	101325	60000	80000	120000				
4	Humidity	fraction	0.7	0	0.1	0.3	0.5	1		
5	Atmospheric molecular weight	kg/kmol	28.9							Not varied since should normally not be changed
Fuel properties										
N	Material name	-	PROPANE	N-HEXANE	N-OCTANE	HEXANE_OCTANE				Use property file 'EXAMPLE_PF' (includes mixture)
6	Material CAS number	-	74986	110543	111659	-20				CAS coupled to material name
7	Combustion efficiency	fraction	1	0.8	0.6	0.4	0.2	0.02	0.001	(WRN) RADFRC reset for COMBEF<0.4 to ensure less than COMBEF; error theory?
8	Specific heat of combustion oxide	J K-1 kg-1	1360	700	2800					
9	Phase for combustion oxide (0-vapour, 1 - nonvapour)	-	0	1						
Pool Data										
10	Temperature	K	231	200	250	300	350			
11	Spill rate (e.g. due to rainout)	kg s-1	4	0.001	0.1	2	8	15.91	20	Bund reached at 15.91 kg/s
12	Elevation of pool fire	m	5	0	10	15	50	100		
13	Is the pool fire on land?	-	TRUE	FALSE						
14	Bund diameter	m	13	6.5149	6.51	3	1	0.1	0.001	Fire diameter = 6.5147 m if no bund
PARAMETERS (values to be changed by expert users only)										
Control of flame-geometry calculation										
15	Calculate flame length & angle?	-	TRUE	FALSE						Two variables below are varied with USECOR=FALSE
16	Input flame length	m	1	18.808	0.01	4.5	40	57	1000	Use basecase flame angle 0.23622 rad. for all variations; (WRN) RADFRC reset <1 for 1000
17	Input flame angle to vertical	radians	0.1	0.23622	0	0.5	1	1.4	1.57	Use basecase flame length 18.808m for all variations

18	**Flame angle method (0 - Johnson, 1 - AGA)**	-	0	1						Also vary windspeed = 0, 0.25,0.5,1,2,4,8,16 (2x8 runs)
19	**Calculate flame diameter?**	-	TRUE	FALSE						Variable below is varied with FNDDIA=FALSE
20	**Input flame diameter**	m	3	6.5147	0.001	0.1	1	60	250	Fire diameter = 6.5147 m if not user-specified
Control of burn rate calculations										
21	**Method of burn rate calculation: 0 - calculate (normal), 1 calculate (ignore max.burn rate in .PRP file), 2 (user-specified)**	-	0	1	2					Variable below is varied with MBCAL=2; consistency between cases is confirmed
22	**Total burn rate**	kg/s	0.1	3.9	0.001	1	80	1000	100000	Use prescribed basecase flame diameter for MBCAL=2; (wrn) RADFRC reset for 0.001
Control of radiation calculations										
23	**Calculate surface emissive power?**	-	TRUE	FALSE						Variable below is varied with FNDPWR=FALSE
24	**Input surface emissive power**	W m-2	4	145027.8	1	100	10000	300000	500000	(wrn) RADFRC reset for 500000
25	**Calculate radiative fraction?**	-	TRUE	FALSE						Varable below is varied with RDFRIN=FALSE
26	**Input radiative fraction**	fraction	0.35	0.340412	0	0.1	0.5	0.7	0.9	0.999 Radiation fraction must be < 1!
Control of output										
27	**Ratio of final axial distance to Froude flame height**	-	1				5	100		
28	**Number of data points**	-	21	2	5	1000	101	201		
29	**ASCII Output (0 = none, 1 = POLF.OUT)**	-	0	1						

Appendix E Detailed information on errors/warnings

Below information on errors/warnings is given

Error messages:

```
2       "Release rate %1%MassFlow% is out of range"
3       "Pool diameter %1%Length% is out of range"
4       "Wind speed %1%Velocity% is out of range"
5       "Flame length %1%Length% is out of range"
6       "Flame angle %1%Angle% is out of range"
7       "Atmospheric temperature %1%Temperature% is out of range"
8       "Atmospheric pressure %1%Pressure% is out of range"
9       "Relative atmospheric humidity %1%real% is out of range"
10      "Atmospheric molecular mass %1%MolecularWeight% is out of range"
11      "Flame elevation %1%Length% is out of range"
12      "Bund diameter %1%Length% is out of range"
15      "Surface emissive power %1%EmissivePower% is out of range"
16      "Radiative fraction %1%real% is out of range"
19      "Modified heat of vaporisation is negative or zero"
20      "Mass burning rate is negative or zero"
22      "Pool diameter is zero"
24      "Air density is negative or zero"
26      "Pool diameter is zero"
28      "Maximum emissive power or emissive power length is out of range"
29      "Output array size %1%integer% is out of range"
30      "Radiative fraction %1%real% must be less than combustion efficiency"
        The radiative fraction is the fraction of energy radiated from the pool fire (W) to total energy
        released by the burned pool(W). This should be smaller than the combustion efficiency, which is the
        mass fraction of fuel which combusts with the surrounding air (combustion efficiency = 1 assumed in
        POLF01).
31      "If user specifies burn rate, he must also specify the flame diameter"
32      "For POLFCF and POLF01 entry point routines, the specified array size must be equal to %1%integer%"
```

Warning messages

```
1001    "Specified liquid pool temperature should not be larger than the liquid boiling
        temperature %1%Temperature%"
        The specified liquid pool temperature should be smaller than the liquid boiling temperature. If it
        erroneously is specified to be larger, it is reset to the liquid boiling temperature.
1005    "One of the mixture components does not have C/H ratio defined and so C/H ratio is assumed to be zero"
        C/H ratio is required for the two-zone pool fire model to estimate clear flame length of the fire. The
        component is assumed to have no carbon if C/H ratio is not specified.
```

NOMENCLATURE

A_t	Combustion reaction parameter, -
C_t	Combustion reaction parameter, -
D	flame diameter, m
D_{bund}	bund diameter (upper bound for flame diameter D), m
D_{Limit}	limit to the early pool fire diameter, m
E_f	surface emissive power of flame, W/m^2
Fr	Froude number
g	gravitational acceleration, m/s^2
H	flame height (Thomas definition), m
H_{fr}	Frounde flame height (at 90% excess air entrainment), m
m_{max}	maximum burn rate of fuel, $kg/m^2/s$
m	burn rate flux of fuel, $kg/m^2/s$
m_F	total burn rate of fuel, kg/s
m_α	mass flow, kg/s; α = tot (total), c (combustion product), entr (entrained excess moist air), oxi (combustion oxides), wi (initial water from stoichiometric air), N2 (nitrogen), unb (unburned fuel), F (fuel); $m_{tot} = m_c + m_{entr}$, $m_c = m_{oxi}+m_{N2}+m_{wi}+m_{unb}$
P_a	atmospheric pressure, Pa
S_{pool}	spill rate of liquid fuel, kg/s
S_{th}	stoichiometric ratio = mass ratio of dry air to fuel needed for complete combustion
S_{thw}	stoichiometric ratio = mass ratio of moist air to fuel needed for complete combustion
T_a	ambient temperature, K
T_b	boiling temperature of liquid fuel, K
u_*	friction velocity, m/s
u_a	ambient wind-speed, m/s
u_{cld}	plume speed, m/s
x	downwind distance, x=0 corresponds to centre of pool, m
y	cross-wind distance, y=0 corresponds to centre of pool, m
z	vertical height above the ground, m
z_{pool}	vertical pool elevation, m

Greek letters

ΔH_c	net heat of combustion of fuel at boilling temperature, J/kg
ρ_m	density of plume, kg/m^3

ρ_a density of ambient air, kg/m^3

ϕ tilt angle of flame (angle to vertical), rad

χ_a combustion efficiency (mass fraction of fuel which burns), -

χ_R radiative fraction (ratio radiated to released energy), -

About DNV

We are the independent expert in risk management and quality assurance. Driven by our purpose, to safeguard life, property and the environment, we empower our customers and their stakeholders with facts and reliable insights so that critical decisions can be made with confidence. As a trusted voice for many of the world's most successful organizations, we use our knowledge to advance safety and performance, set industry benchmarks, and inspire and invent solutions to tackle global transformations.

Digital Solutions

DNV is a world-leading provider of digital solutions and software applications with focus on the energy, maritime and healthcare markets. Our solutions are used worldwide to manage risk and performance for wind turbines, electric grids, pipelines, processing plants, offshore structures, ships, and more. Supported by our domain knowledge and Veracity assurance platform, we enable companies to digitize and manage business critical activities in a sustainable, cost-efficient, safe and secure way.

DNV | digital@dnv.com | dnv.com/digital

REFERENCES

[1] Mudan, K.S., “Fire hazard calculations for large open hydrocarbon fires”, Section 3-11 in “SFPE handbook of fire protection engineering”, Second Edition, National Fire Protection Association, Quincy, MA (1995)
[2] Rew, P.J., Hulbert, W.G., and Deaves, D.M., “Modelling of thermal radiation from external hydrocarbon pool fires”, Trans. IchemE 75, Part B, pp. 81-89 (1997)
[3] “Handbook on fire calculations and fire risk assessment in the process industry”, SINTEF, Norway (1992)
[4] Engelhard, W.F.J.M., “Heat flux from fires”, Ch. 6 in “Methods for the calculation of physical effects”, CPR14E, Part 2 (TNO Yellow Book), SDU Uitgevers, The Hague (1997)
[5] DNV, “SAFETI software for the assessment of flammable explosive and toxic impact - Theory Manual”, Version 3.4, DNV, London, November 1996
[6] Cook, J., Bahrami, Z., and Whitehouse, R.J., “A comprehensive program for calculation of flame radiation levels”, Proceeding of First Int. Conf. on Loss of Containment, London, UK (1989) and (??) J. Loss Prev. Process Ind. 3, pp. 150-155 (1990)
[7] “PHAST Version 4.2 release notes”, DNV, December 1993
[8] Witlox, H.W.M., Woodward, J.L., Rowley, M.E., and Sharvanandhan, K., “Modelling of phosphorus fires with hydrolysis in the plume”, pp. 1100-1111 in “Proceedings of 9th Int. Symposium on Loss Prevention and Safety Promotion in the Process Industries”, Barcelona, May 1998
[9] Witlox, H.W.M. and Woodward, J.L.,”Modelling of phoshorus pool fires and subsequent dispersion of combustion products with hydrolysis in the plume”, Contract C755300 for Albright and Wilson, DNV, London (1997)
[10] Delichatsios, M.A., “Air entrainment into buoyant jet flames and pool fires”, Section 3-2 in “SFPE handbook of fire protection engineering”, Second Edition, National Fire Protection Association, Quincy, MA (1995)
[11] Witlox, H.W.M., “Modelling of kerosene fire and smoke dispersion following Bijlmermeer aeroplane crash”, Contract C480041 for RIVM, DNV, London (1998)
[12] Daubert, T.E. and Danner, R.P., “Physical and thermodynamic properties of pure chemicals; data compilation (DIPPR handbook)”, Design Institute for physical property data, American Institute of Chemical Engineers, Taylor and Francis, Washington (1996)
[13] Chemical Safety Data Sheet, ???????
[14] Burgess, D. and Hertzberg, M., “Radiation from pool flames”, Chapter 27 in “Heat transfer in flames” (eds. Afgan, N.H. and Beer, J.M.) (1974)
[15] Thomas, P.H., “The size of flames from natural fires”, 9th Int. Combustion Symposium, Comb. Inst., Pittsburgh, PA, pp. 884-859 (1963)
[16] American Gas Association (AGA), “LNG safety research program”, Report IS-3-1 (1974)
[17] Johnson, A. D. “A model for predicting thermal radiation hazards from large-scale LNG pool fires”, IChemE Symp. Series 130,pp. 507-524 (1992)
[18] Koseki, H., Large scale pool fires: results of recent experiments. Fire Safety Science – Proceedings of the 6th international symposium, 2000
[19] Pritchard, M.J. and Binding, T.M., Fire2: a new approach for predicting thermal radiation levels from hydrocarbon pool fires. IChemE symposium series No. 130, 1992
[20]Sharvanandhan, K. and Rowley, M.E., Private Communication and “Consequence analysis for phosphorus fires”, Handout by Albright&Wilson (1997)
[21] Wayne, F.D., “An economical formula for calculating atmospheric infrared transmissivities”, J. Loss Prev. Process Ind. 4, pp. 86-92 (1991)
[22] Harper, M., “Modelling for calculating radiation exposure”, DNV, London (2003)
[23] Nedelka, D., Moorhouse, J., and Tucker, R. F., “The Montoir 35m diameter LNG pool fire experiments” Proc. 9th Intl. Cong and Exposition on LNG, LNG9, Nice, 17-20 October 1989, Published, Institute of Gas technology, Chicago, Vol. 2, pp III-3 1-23 (1990)
[24] Lois, E., and Swithenback, J., “Fire hazards in oil tank arrays in a wind”, Colloquium on fire and explosion, pp 1087-1098 (?????)
[25] McCaffrey, “Flame Height”, Section 1-2 in “SFPE handbook of fire protection engineering”, Second Edition, National Fire Protection Association, Quincy, MA (1995)